71-12,990

SHEPARD, Kenneth Wayne, 1941-
MICROWAVE ENHANCED SUPERCONDUCTIVITY.

Stanford University, Ph.D., 1970
Physics, solid state

University Microfilms, A XEROX Company, Ann Arbor, Michigan

THIS DISSERTATION HAS BEEN MICROFILMED EXACTLY AS RECEIVED

MICROWAVE ENHANCED SUPERCONDUCTIVITY

A DISSERTATION

SUBMITTED TO THE DEPARTMENT OF PHYSICS

AND THE COMMITTEE ON GRADUATE STUDY

OF STANFORD UNIVERSITY

IN PARTIAL FULFILLMENT OF THE REQUIREMENTS

FOR THE DEGREE OF

DOCTOR OF PHILOSOPHY

By

Kenneth Wayne Shepard

August 1970

I certify that I have read this thesis and that in my opinion it is fully adequate, in scope and quality, as a dissertation for the degree of Doctor of Philosophy.

William A. Little

(Principal Adviser)

I certify that I have read this thesis and that in my opinion it is fully adequate, in scope and quality, as a dissertation for the degree of Doctor of Philosophy.

Alexander L. Fetter

I certify that I have read this thesis and that in my opinion it is fully adequate, in scope and quality, as a dissertation for the degree of Doctor of Philosophy.

H.A. Schwettman

Approved for the University Committee on Graduate Studies:

Lincoln T. Moses

Dean of the Graduate Division

PREFACE

This dissertation describes work done at Stanford University over the period 1966 to 1970, under the direction of Professor W. A. Little.

The work is a study of the microwave properties of superconducting aluminum thin films.

The films were scribed into narrow strips which displayed a dipole antenna-like resonance when irradiated with microwaves over a wide frequency range.

We constructed a tunable mm wave source, an electron cyclotron maser, which provides several milliwatts of power over the frequency range 30-128 GHz. To measure the dipole response we constructed a low temperature Germanium microwave bolometer, usable over a broad frequency range.

The dc critical current of the thin films was in good accord with the value predicted by the B.C.S. theory. The microwave response was measured by the effect of microwave radiation on the dc critical current.

We have observed a microwave induced increase of the dc critical current, in some respects similar to the Wyatt* effect.

The frequency dependence of the microwave enhancement of critical current is suggestive of a relationship between the dipole resonance and the enhancement. A model is proposed.

Some earlier results of the study have been published in the Proceedings of the International Conference on the

Science of Superconductivity, Stanford, California, 1969.

This work was supported by the Office of Naval Research and by the Advanced Research Projects Agency through the Center for Materials Research at Stanford University.

I would like to thank I. B. Bott, of the Royal Radar Establishment, Malvern, and J. P. Beasely of Mullard Ltd., for providing helpful information about the construction of the electron cyclotron maser, D. K. Rose for advice on thin film techniques and the loan of much equipment, and G. E. Possin with whom I collaborated on a low-frequency measurement of kinetic inductance.

I especially thank Professor W. A. Little, who suggested this experiment, for his encouragement and advice.

Finally, I thank my wife Barbara, for enduring many years as a graduate student wife.

*A.F.G. Wyatt et al., Phys. Rev. Letters 16, 1166 (1966).

TABLE OF CONTENTS

		Page
PREFACE		iii
LIST OF FIGURES		vii
LIST OF TABLES		viii
CHAPTER		
I.	INTRODUCTION	1
	A. Background	1
	B. Principal Features of the Experiment	2
	1. The System Studied	2
	2. The Apparatus	5
	C. Principal Results	6
II.	THE MICROWAVE GENERATOR	7
	A. Background	7
	B. The Electron Cyclotron Maser Tube	9
	C. The Superconducting Magnet	10
	D. The Magnet Dewar	12
	E. Low Field Magnets	14
	F. Operation and Performance	16
	G. Microwave Optics	19
III.	SAMPLE PREPARATION AND APPARATUS	22
	A. Thin Film Aluminum Dipoles	22
	B. Sample Dewar	25
	C. The Bolometer	28
	D. Electronics	31

IV. RESULTS AND DISCUSSION 33
A. Features of the I-V Curves 33
B. dc Behavior of the Superconducting Films 35
1. The Resistive Transition 35
2. Theoretical Penetration Depth 37
3. The dc Critical Current 39
C. The Microwave Response of the Dipoles ... 43
1. Theoretical Response--The Half-wave Line 43
2. The Impedance of the Superconducting Strip 46
3. The Experimental Microwave Response 51
D. Microwave Enhanced Critical Currents 54
1. Introduction 54
2. The Observed Phenomena 57
3. A Model for Microwave Enhanced Superconductivity 59
V. CONCLUSION 68
REFERENCES 69

LIST OF FIGURES

		Page
1.	Thin aluminum film folded dipole	3
2.	The electron cyclotron maser	8
3.	Cross section of the superconducting solenoid	11
4.	Cross section of re-entrant dewar	13
5.	The corkscrew solenoid	15
6.	ECM electronics	17
7.	ECM output spectrum	18
8.	Block diagram of the millimeter wave optics	20
9.	Thin film sample geometry	23
10.	Sample dewar insert	27
11.	Cross section of microwave bolometer	29
12.	Bolometer circuit and response	30
13.	The experimental set-up	32
14.	Structure of the I-V curves	34
15.	Typical resistive transition	36
16.	dc critical current vs. temperature	42
17.	Transmission line model for dipole microwave response	44
18.	Two fluid impedance model	47
19.	Effective inductance vs. temperature	50
20.	Dipole microwave response	52
21.	dc critical current vs. microwave power	55
22.	Free energy vs. order parameter	64
23.	$(dI_c/dP)_{p=0}$ vs. ω	65

LIST OF TABLES

Page

1. Comparison of observed and predicted resonant frequencies in superconducting dipoles 53

CHAPTER I

INTRODUCTION

A. Background

The experiment described is an investigation of the effects of low-frequency plasmon excitations on superconductivity. Except for some work on charge density oscillations in Josephson junctions,[1] no previous experiments have been reported, possibly because of general acceptance of Anderson's assertion that plasmons are unimportant in superconductivity since plasmon excitation energies are much larger than the superconducting energy gap.[2]

Onsager[3] pointed out a possible exception to this case in a cryptic comment on Little's[4] proposed superconducting polymer:

> "While the superfluid transition of the He is sharpened by particle interaction, the energy gap remains "punctured" by the phonic excitations. Schafroth pointed out that a set of charged Bosons would have a finite smallest energy of excitation--essentially a plasma frequency. The unpunctured energy gap of a superconductor exists because the excitations become baby plasmons.
>
> However, in order to get a plasma frequency you need a set of particles whose interaction potential satisfies Laplace's field equation in the number of dimensions filled by the array of particles. A one-dimensional system of three-dimensional electrons does not qualify."

Onsager seems to have suggested that in a one-dimensional superconducting system there exist low-frequency plasma excitations "puncturing" the superconducting energy gap, possibly destroying any superconductivity.

While the validity of Onsager's criticism of molecular superconductivity is not entirely clear, a question is raised as to the effects of a collective excitation within the energy gap of a superconductor.

Low-frequency plasmons exist in any finite piece of metal. These are shape resonances, at frequencies determined primarily by the metallic geometry. For example, in a television antenna, as in any long conducting cylinder, the lowest energy plasmon excitation corresponds to a half-wave resonant, dipole charge-density oscillation.

The experiment undertaken was to study the properties of metallic thin-film superconducting dipoles of resonant frequency comparable to the gap frequency. The objects were to observe the dipole resonance and any effects on the superconducting state.

B. Principal Features of the Experiment

1. The System Studied

The experiment was to excite high-frequency charge density oscillations in a narrow superconducting strip with microwave radiation while simultaneously measuring the dc critical current.

The system studied was thin (20-100Å) aluminum films scribed into the folded dipole geometry shown in Figure 1. This geometry was used to allow four-terminal superconducting contacts to be made to a narrow strip without interfering with the high-frequency dipole resonance.

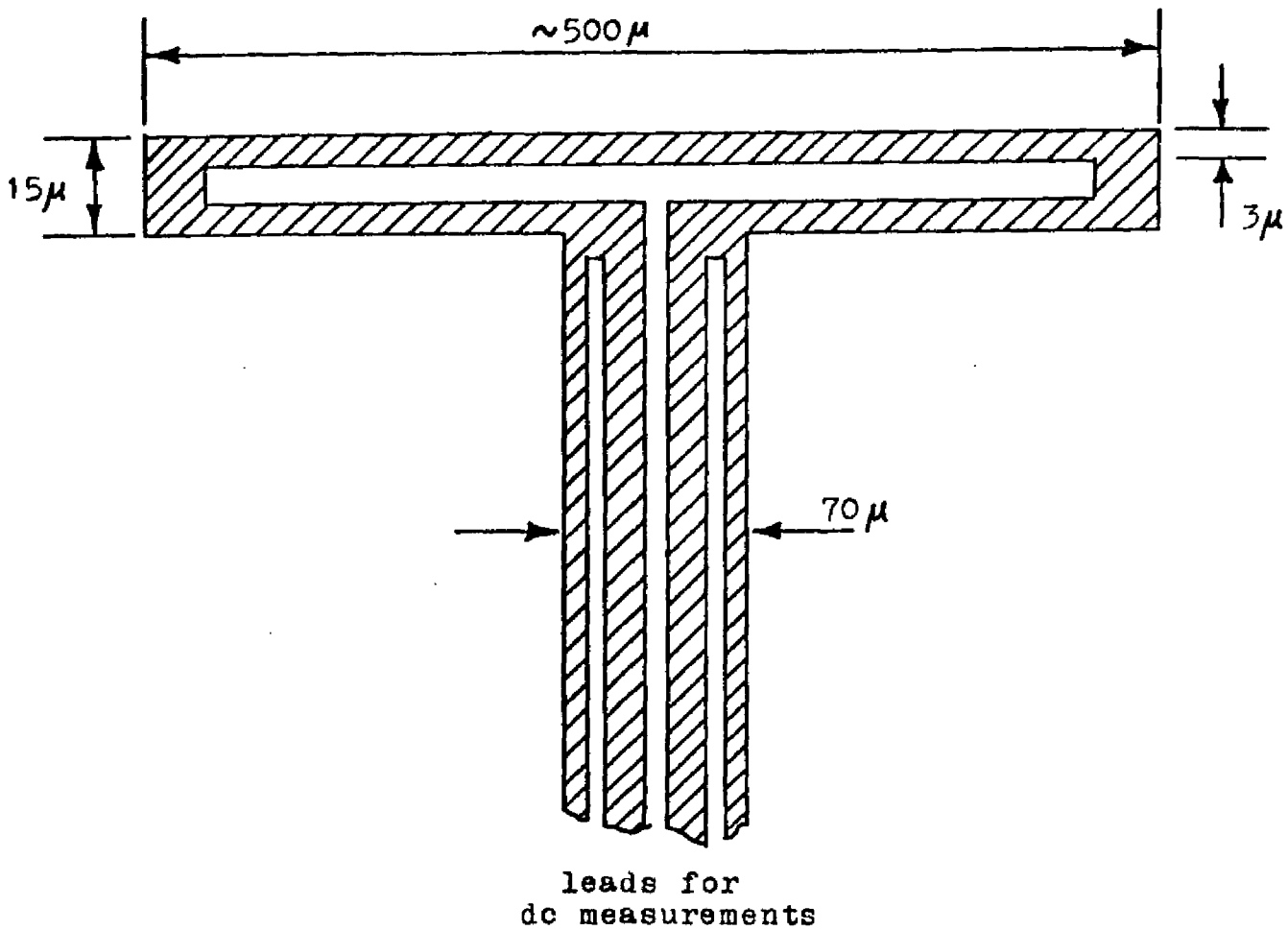

Figure 1. Thin aluminum film folded dipole. The aluminum films were typically 30Å thick.

In order to approximate the electrodynamics of a superconducting polymer, the cross sectional area A of the dipole strips was made as small as possible, $O(10^{-10}\ cm^2)$, so that $(\lambda^2/A) > 1$, where λ is the penetration depth in the aluminum film. In this case, the impedance of the strip is determined primarily by the kinetic inductance L_K of the superfluid[5,6] which is larger than the magnetic inductance by a factor λ^2/A.

The kinetic inductance represents the inertia of the superelectrons in an ac field and can be obtained from the accelerative London equation

$$E = \mu_0 \lambda^2 \frac{\partial J_s}{\partial t} \qquad (I\text{-}1)$$

relating the supercurrent J_s to the electric field E. Assuming $\exp(i\omega t)$ time dependence, and a uniform current distribution, I-1 becomes

$$E = i\omega(\mu_0 \lambda^2/A)I \ , \qquad (I\text{-}2)$$

showing that the impedance of the superconductor can be expressed as a kinetic inductance,

$$L_K = \mu_0 \lambda^2/A \ . \qquad (I\text{-}3)$$

The microwave properties of the folded dipole can be approximated by considering either the top or bottom strip as a transmission line of capacitance C and inductance L per unit length. For a line of length ℓ, the lowest frequency

charge-density excitation is at a frequency $\omega_1 = (\pi/\ell)(LC)^{-\frac{1}{2}}$.

Ordinarily, C and L scale with the cross section of a long metallic cylinder in such a way that the product LC remains constant, and the phase velocity along the line is always equal to the velocity of light. In this case the resonant frequency corresponds to a wavelength 2ℓ, and the half-wave resonance of the line depends only upon the length.

For the superconducting dipoles the resonant frequency depends upon the kinetic inductance, which in turn depends upon the degree of condensation into the superconducting state. In the system studied, the frequency of the charge density excitation is directly coupled to the superconducting order parameter.

The small cross-sectional areas of the dipole strips also enable direct measurement of the condensation energy. This occurs for two reasons. In the limit $(\lambda^2/A) > 1$, any supercurrent is uniformly distributed across the strip[7] so that the critical current density is known. Also, for $(\lambda^2/A) > 1$, the self-field of a critical supercurrent is insufficient to produce vortices within the strip,[8] so that in the absence of an external magnetic field, the dc critical current is determined by depairing[9] rather than flux-flow heating.

2. The Apparatus

In order to observe the dipole resonance a mm wave source tunable over a broad frequency range was required. We con-

structed an electron cyclotron maser, of the sort devised by Bott,[10] which operates over a range of 30-128 GHz.

Power levels were measured with a germanium bolometer in the same dewar as the dipole. Microwave radiation was polarized with E parallel to the dipole and precautions were taken to eliminate effects due to standing waves within the film substrate and within the apparatus.

The microwave output was in the form of 500 μs pulses and the dc critical current was measured with a sawtooth current pulse used to trace the I-V characteristic of the dipole while the microwaves are on. The dc critical current was measured as a function of microwave power at various frequencies and temperatures.

C. Principal Results

The dipoles studied exhibited a resonant microwave response with temperature and frequency dependence in quantitative agreement with the accepted electrodynamics of superconductors.

The dc critical current agreed well with the B.C.S. theoretical value. Under some conditions, the presence of a microwave field increased the dc critical current of the dipoles. This unusual effect suggests an interaction between the microwave field and the superconductor which increases the condensation energy of the superconducting state. We have obtained some evidence, discussed at length in section IVD, that such an interaction is provided by the dipole resonant charge density oscillations.

CHAPTER II

THE MICROWAVE GENERATOR

We describe the principles of operation of the electron cyclotron maser, the vacuum tube constructed, and the magnets and associated equipment required for operation.

A. Background

In 1965, I. B. Bott[10] constructed a tunable mm wave generator. This device followed theoretical predictions of stimulated emission of radiation at the cyclotron resonance frequency by weakly relativistic electrons in a strong magnetic field.[11,12]

The relativistic change of cyclotron resonance frequency with electron kinetic energy removes the degeneracy of energy level spacing for electrons in a magnetic field and a detailed calculation shows that stimulated emission is possible.[11]

A schematic of the electron cyclotron maser (E.C.M.), is shown in Figure 2. A pulsed beam of approximately 60 mA at 20 kV emerges from the gun and passes through a region with an axial magnetic field of 500 G. In this region a transverse perturbing field of a few gauss is applied. Moving along the tube axis, the direction of the transverse field rotates. The effect of the "corkscrew" perturbing field on the electron beam is to produce a transverse velocity component;[13] the electrons assume helical trajectories as they proceed towards the strong field region, 12-42 kG, at the cavity end of the

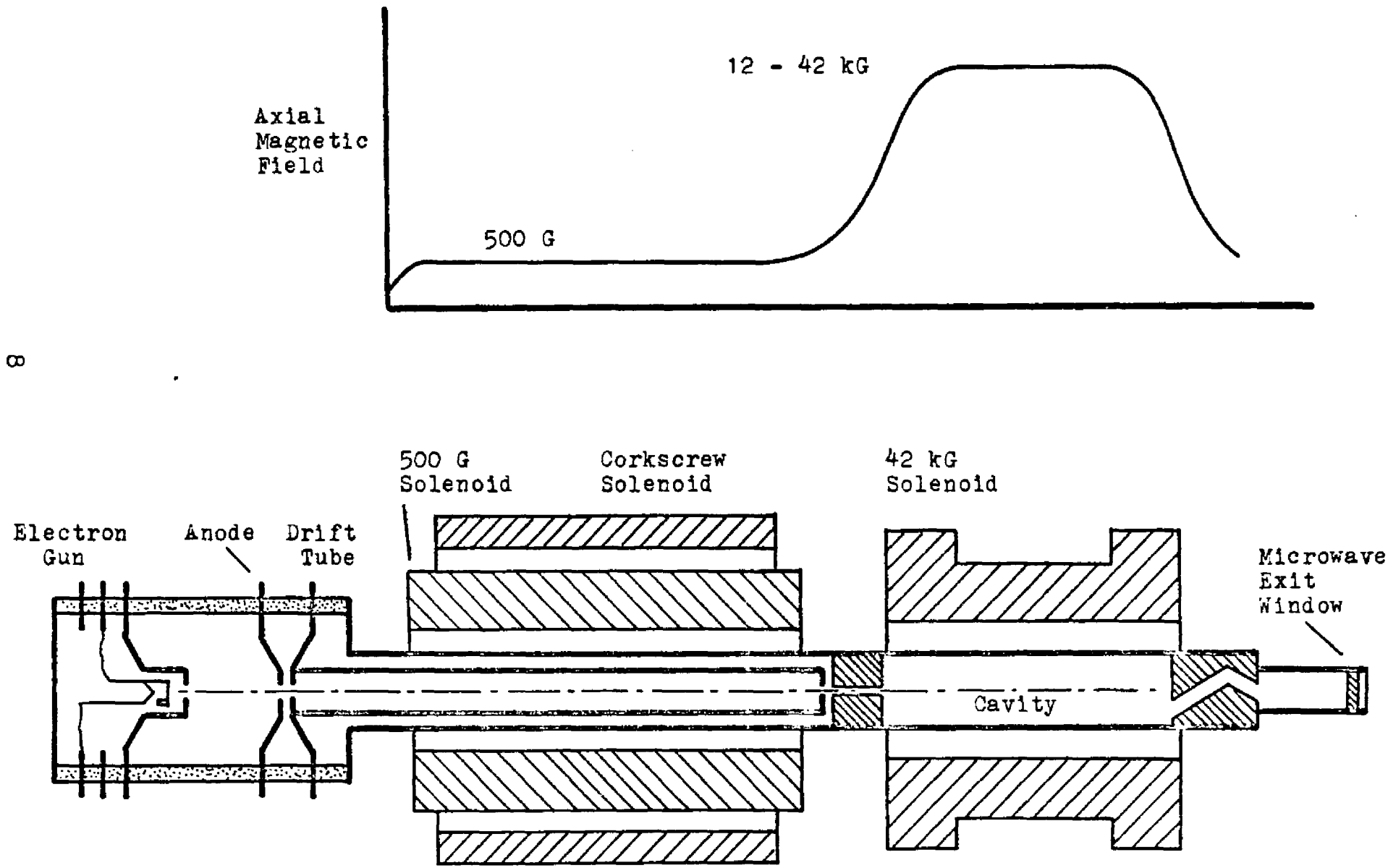

Figure 2. The Electron Cyclotron Maser.

tube. Upon entering the strong field region, the transverse velocity is greatly increased.

In operation, the corkscrew field is adjusted so that about one quarter of the incident beam is reflected from the magnetic mirror of the strong field region. The remaining electrons enter the cavity with a high percentage of kinetic energy in the cyclotron orbital motion.

The cavity dimensions are many wavelengths long at the frequencies used, so there are a number of closely spaced modes near the cyclotron resonance frequency. When the magnetic field is adjusted so that the cyclotron resonance coincides with a mode of the cavity, oscillation occurs.

At the end of the cavity is a sapphire window through which the mm wave power is coupled to a waveguide.

B. The Electron Cyclotron Maser Tube

Mr. J. A. McGowan of the Stanford Electronic Research Laboratories Tube Shop both constructed the tube and provided much of the design. The gun housing consists of ceramic tubes brazed to cupro-nickel rings which provide electrical contact to the cathode, heater and various anodes. The remainder of the tube is housed by a 3/4" stainless steel tube.

For the first portion of the electron gun we used the "Stanford $\frac{1}{2}$" Gun Layout", a standardized design. Since pulsed operation is used the anode of this gun provides a control grid to which the driving pulse is applied. We used a 3 mm cathode and designed for a perveance of 1.5×10^{-6}

$A/V^{3/2}$. A driving pulse of 1200V provides a beam current of 60mA. Higher currents can be obtained, but are not necessary for operation of the tube.

The next two anodes focus and accelerate the beam to 20 kV and it enters a drift tube to pass through the corkscrew field region. The portion of the beam not entering the cavity is collected by the drift tube and can be measured, since the drift tube is electrically isolated from the cavity. Measurement of the drift tube current allows the electron optics to be checked out and is used during operation of the tube in adjusting the corkscrew field for partial reflection of the beam.

The cavity consists of two copper end blocks enclosing a six inch length of the stainless steel housing tube with 1 mil of copper electroplated onto the inside surface. The final end block has an offset radiation exit so that the electron beam is absorbed in the copper without damaging the sapphire exit window.

C. The Superconducting Magnet

To obtain the high magnetic fields required for electron cyclotron frequencies in the mm wave region a superconducting solenoid was constructed. A cross section of the magnet is shown in Figure 3.

The winding consists of 10,000 feet of Supercon A-25 wire, a Niobium -25% Zirconium alloy of 10 mil diameter with a 1.5 mil coating of copper to improve thermal stability. Each layer is interleaved with 1/2 mil mylar sheet for electri-

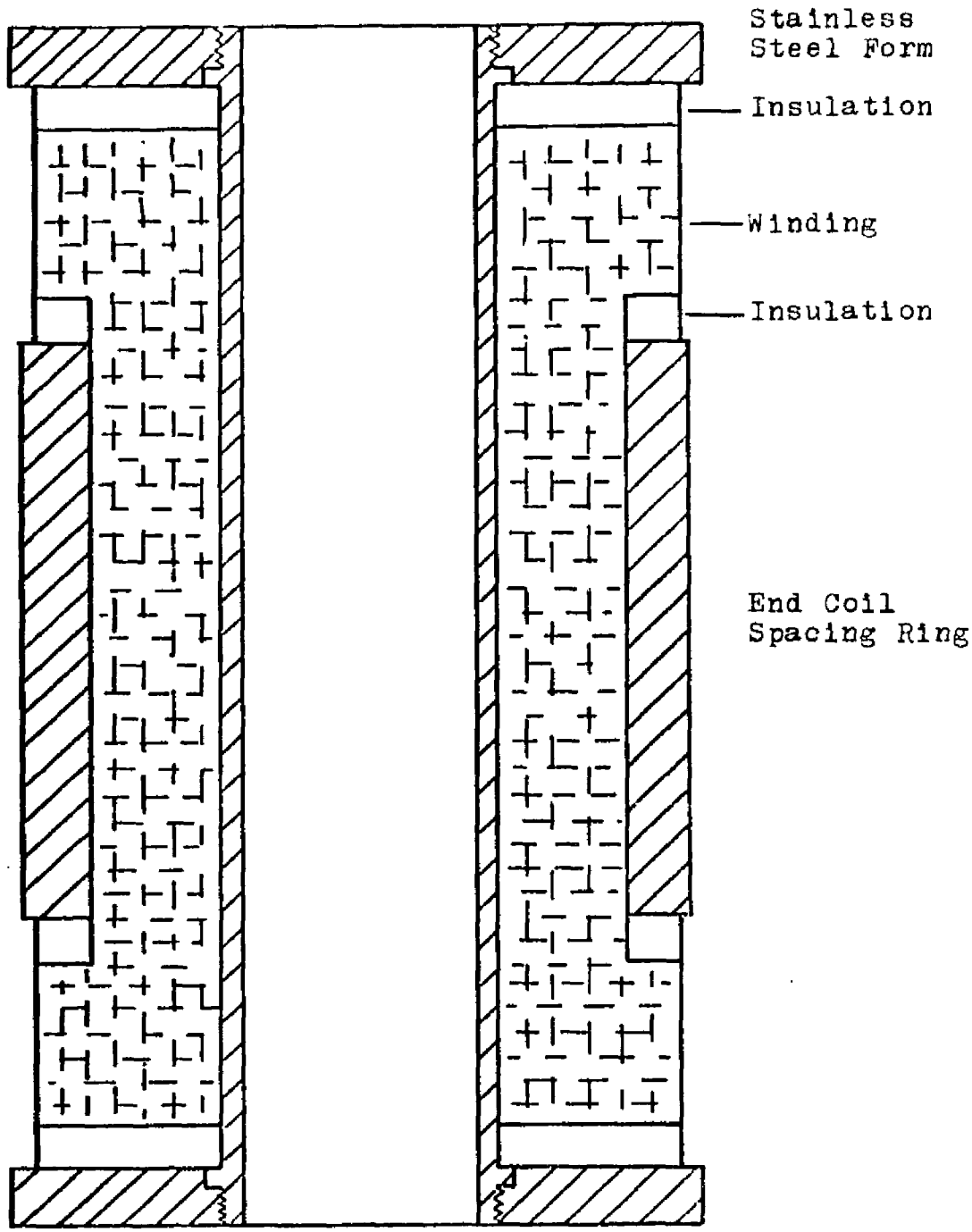

Figure 3. Cross section of the superconducting solenoid. Shown full size.

cal insulation and every fifth layer interleaved with 2 mil copper sheet to facilitate cool-down of the winding.

The winding form is a heavy stainless steel spindle used to reduce deformation of the form by tension in the winding. An end coil correction was computer designed to optimize field uniformity over a 4 cm. length at the center of the bore.

A superconducting switch was placed across the input leads of the magnet to allow operation in a persistent mode. The switch consists of 1 m of superconducting wire potted in epoxy along with a heating wire. The switch is connected to the input leads with an indium solder joint. Since this is not a superconducting joint the magnet is not truly persistent but has a decay time of about 10^6 seconds with the shunt superconducting.

The magnet has been energized to 46 kG and can be energized to 42 kG without danger of quenching. The short sample wire characteristics predict a maximum field of 52 kG so the achieved performance is quite satisfactory. The magnet has been quenched repeatedly without damage.

The field uniformity has not been measured but a calculation from actual winding dimensions predicts 0.1% uniformity over the central 4 cm length of the accessible bore region.

D. The Magnet Dewar

To allow room-temperature access to the 40 kG field, a reentrant helium dewar was built with a room temperature

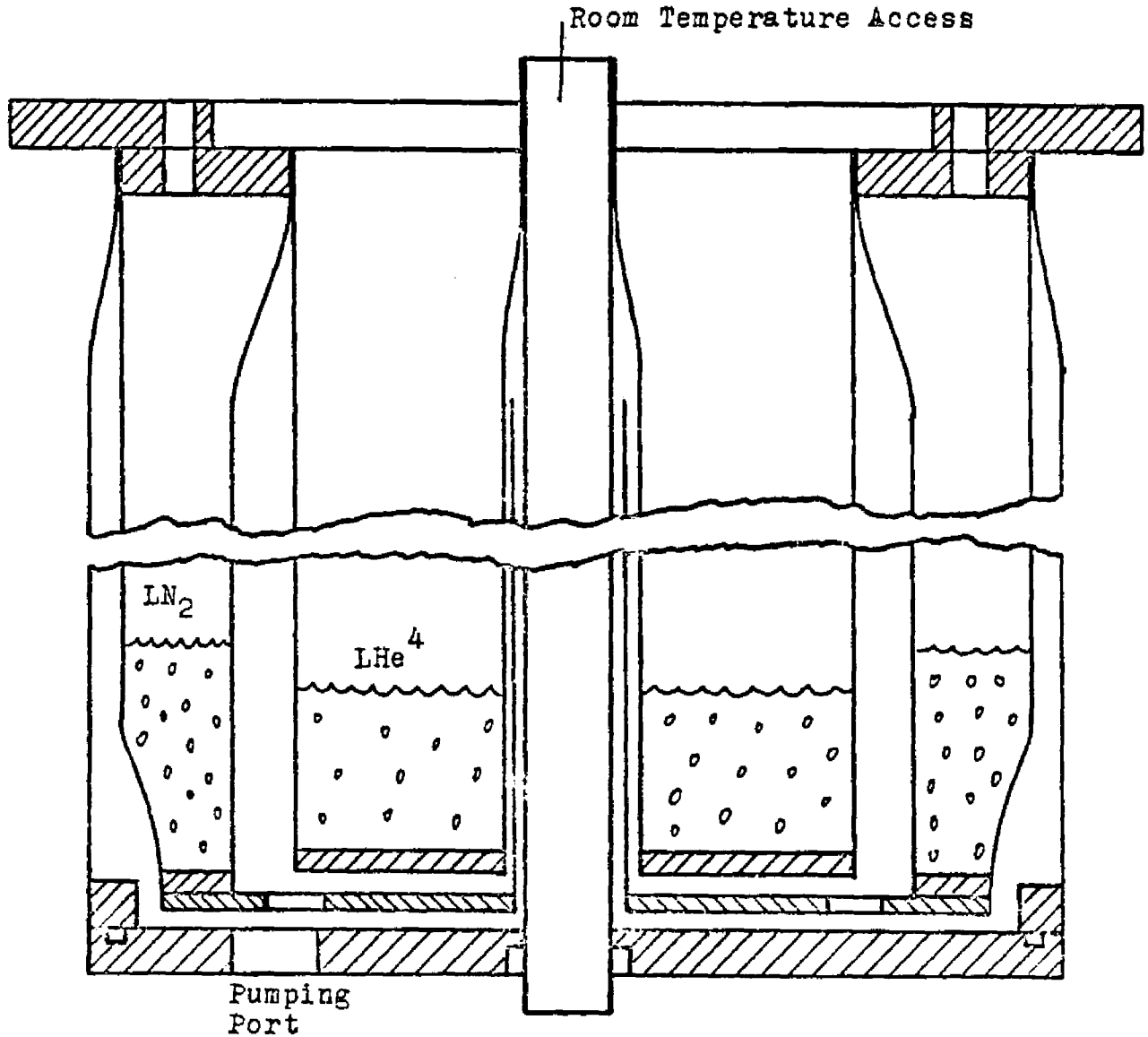

Figure 4. Cross section of re-entrant dewar. Shown 5/8 scale. A radiation shield is thermally tied to the bottom of the liquid nitrogen well.

access hole through the center. A cross section of the magnet dewar is shown in Figure 4.

Construction was of stainless steel tubing, spun to the required shapes and arc-welded. The vacuum was maintained by continuous pumping.

Six layers of aluminized Mylar super-insulation were wrapped inside and outside the liquid nitrogen temperature radiation shield around the access hole. Although a nylon net was used to space successive layers of super-insulation, the available space was quite limited and the super-insulation was very tightly wrapped. It was feared that consequent thermal conduction between adjacent layers would impair the radiation shielding, but the shielding proved satisfactory.

The liquid nitrogen loss rate was inconveniently high until five layers of super-insulation were placed between the outer wall and the nitrogen well.

The dewar holds six liters of liquid helium with a loss rate of 0.2 liter/hour. Copper leads required to carry current to the magnet increase the loss to 0.3 liter/hour.

E. Low Field Magnets

The 500 G axial field was provided by a copper solenoid nested inside the corkscrew solenoid. Compressed air was forced between the two for cooling.

The corkscrew magnet is shown in Figure 5. The bifilar winding produces a transverse field component in a direction rotating with the pitch of the winding.[13] The pitch was

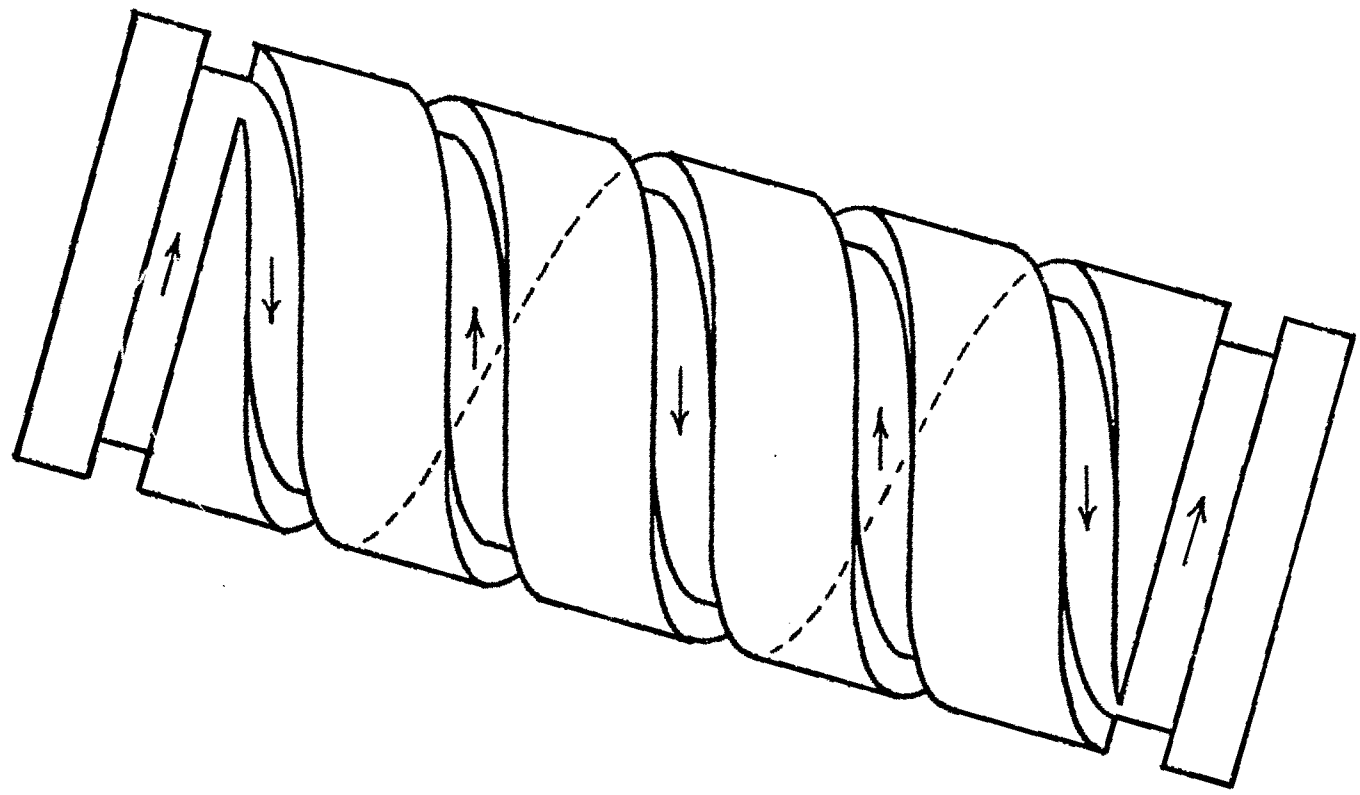

Figure 5. The corkscrew solenoid. The bifilar winding lays in a double thread on an aluminum form. Direction of current flow is shown by the arrows and produces a corkscrewing transverse field component.

chosen so that a 20 kV electron moving along the axis sees a transverse field rotating at the cyclotron resonance frequency of the 500 G axial field. The electron assumes a helical trajectory with a diameter controlled by the current through the corkscrew solenoid.

F. Operation and Performance

Figure 6 is a block diagram of the E.C.M. apparatus.

The low field and corkscrew solenoids were powered by adjustable current regulated supplies. A 0-30A current regulated power supply was constructed for the superconducting solenoid.

The high voltage supply was a Plastic Capacitors Inc. Power Pack delivering 2 mA at 30 kV. The output voltage could be varied from 0-30 kV by adjusting the ac input to the supply. A 1.0 μF capacitor was placed across the HV output to provide the 60 mA current pulses required for the E.C.M. beam.

A driving pulse generator provided 1200 V, 500 μsec pulses for turning on the E.C.M. beam and a trigger pulse for the oscilloscopes used. A repetition rate of about 20 pulses/sec was used.

The output frequency of the E.C.M. is determined by the magnetic field strength at the cavity. To operate the E.C.M. the current to the superconducting solenoid is set at a value corresponding to the desired frequency. The low field and corkscrew solenoid currents are then adjusted so that about

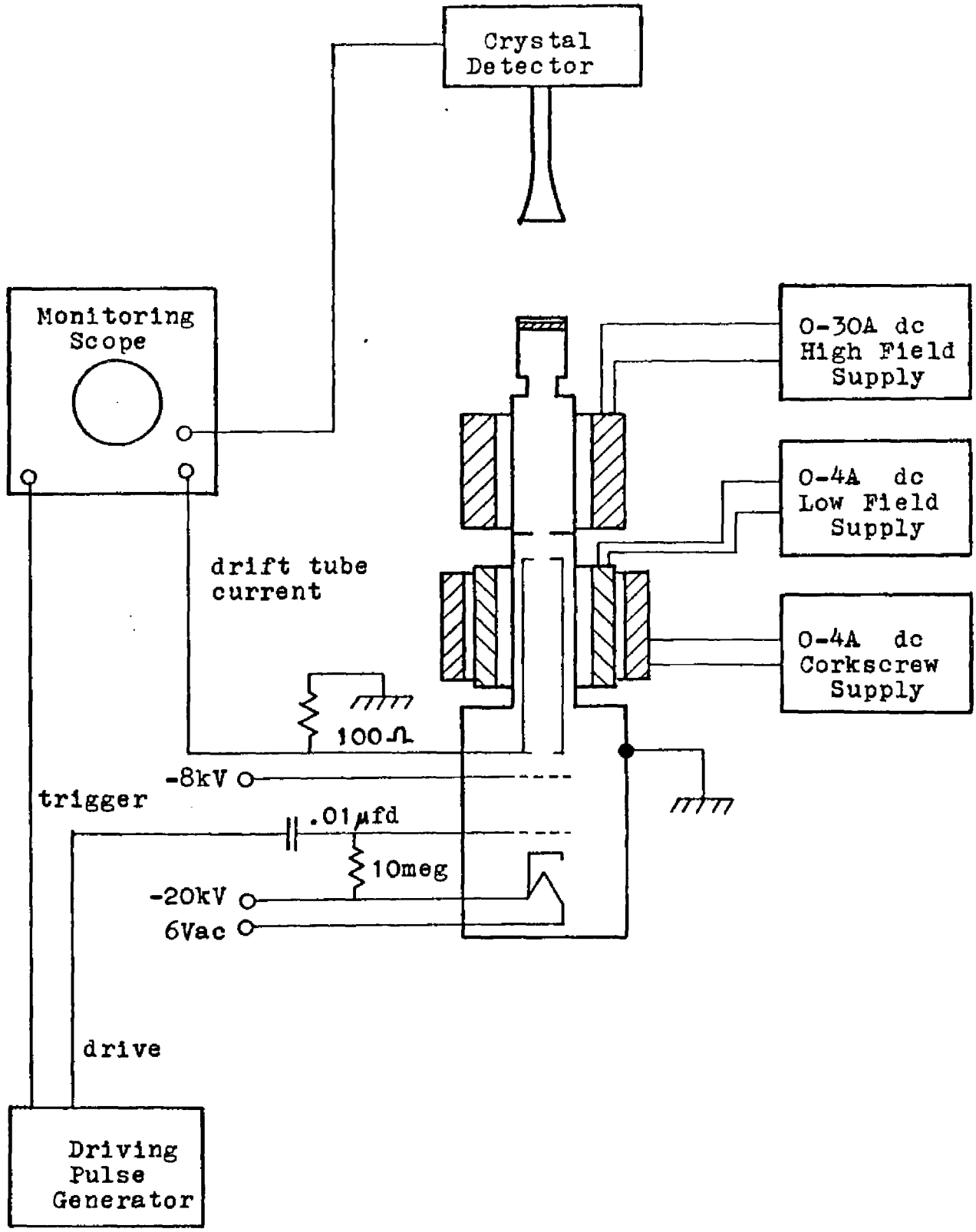

Figure 6. ECM electronics.

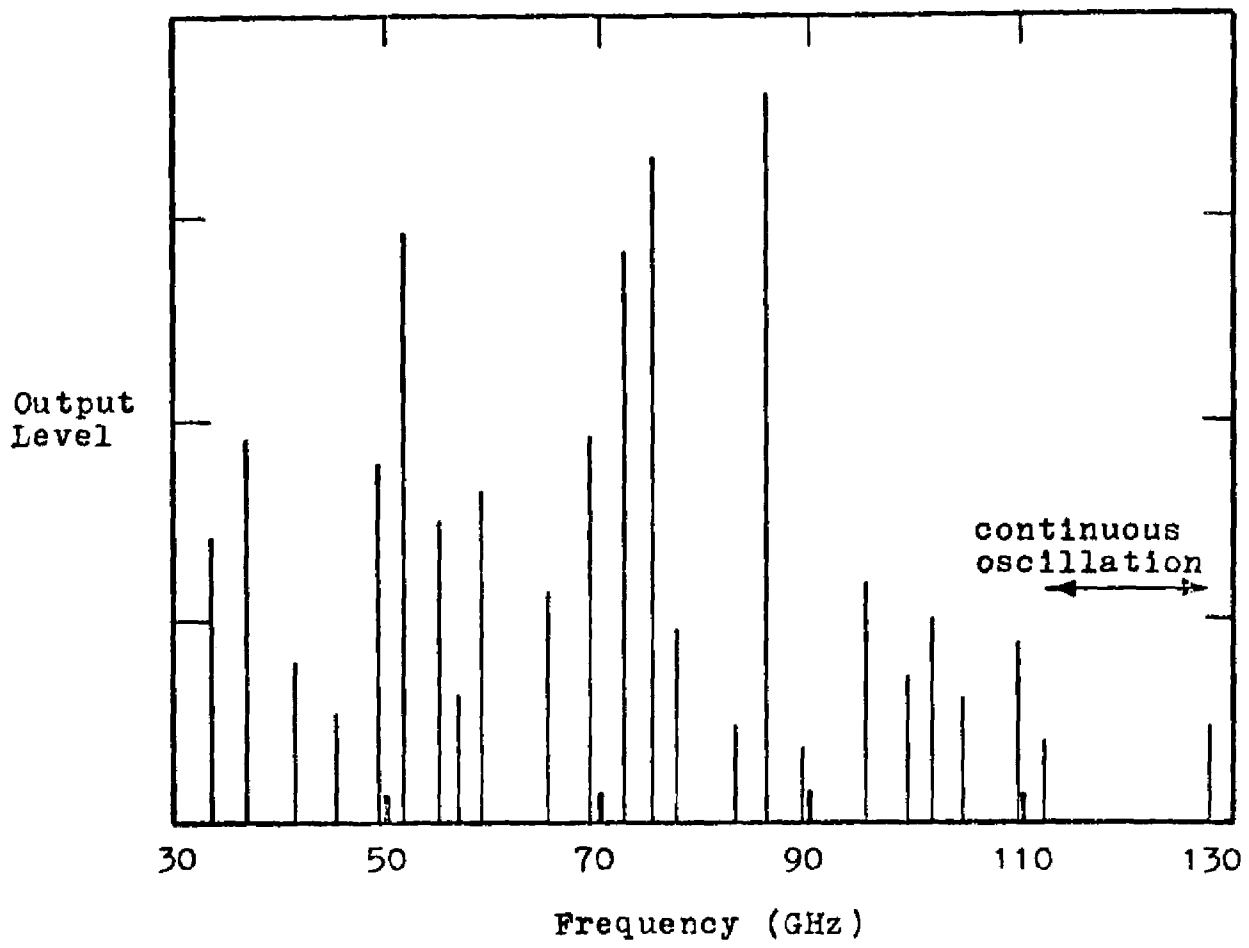

Figure 7. ECM output spectrum. Only the strongest lines are shown. The maximum output levels are on the order of a few milliwatts.

75% of the electron beam enters the cavity, the remainder being reflected. The E.C.M. output is monitored with a crystal detector and the cavity field is varied until oscillations are obtained. Fine adjustments of all three solenoids are then made to obtain a uniform (square) output pulse.

The output is not continuously tunable but consists of a series of closely spaced lines, shown in Figure 7. Only the principle lines are shown, for which the output levels are on the order of a few milliwatts.

The highest frequency obtained, 128 HGz, is limited by the maximum field of the superconducting magnet. With a 100 kG magnet, frequencies of 284 GHz could be achieved.

G. Microwave Optics

Figure 8 schematizes the microwave optics used.

Copper tubing of $\frac{1}{4}$" i.d. was used as a circular waveguide. For waveguide into the sample dewar $\frac{1}{4}$" stainless steel tubing was used to minimize heat leaks. The steel waveguide was gold plated on the inside to reduce microwave losses.

The lowest frequency used in the experiment, 33 GHz, is the cutoff frequency of the waveguide. At the highest frequencies used, 110 GHz, propagation in the guide is possible in eleven different modes. The mode of propagation must be known in order to determine the microwave field strength at the superconducting dipole.

The TE_{11} mode in circular guide has the lowest cutoff

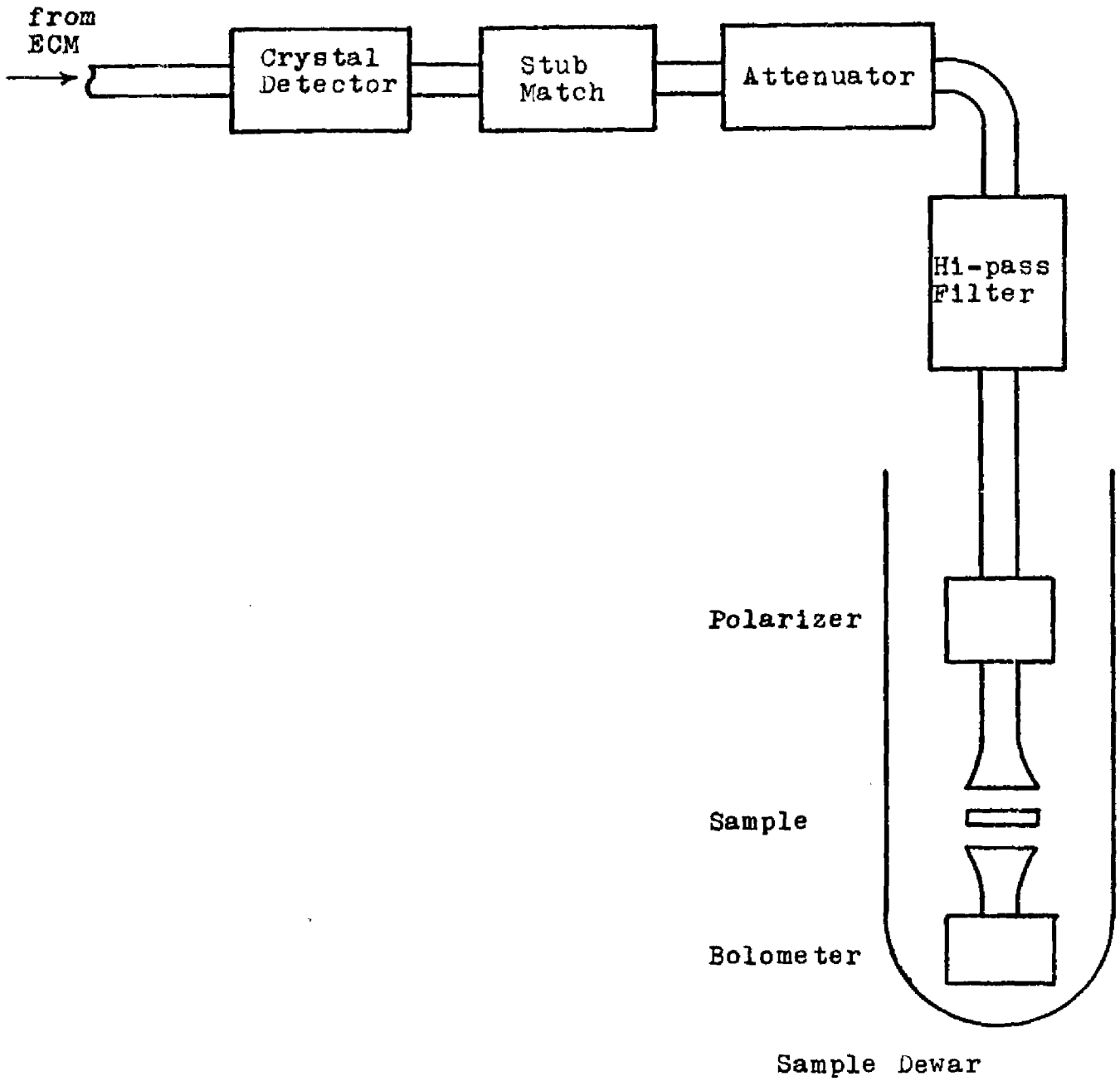

Figure 8. Block diagram of the millimeter wave optics.

frequency and the simplest field distribution of any mode. To insure propagation in the TE_{11} mode, constricted sections of waveguide were inserted to reflect other modes. The output of the E.C.M. was found to be predominantly in the TE_{11} mode at all frequencies.

Microwave polarization was determined by a grid of wires inserted into the waveguide which reflected unwanted components of polarization.

A stub match was used to maximize power to the bolometer. Power levels were controlled with an attenuator made from Eccosorb MF-114 ferrite microwave absorber which was found to perform well at mm wavelengths.

The crystal detector consisted of a type IN-23c X-band microwave crystal inserted through the waveguide. While the crystal detected microwaves satisfactorily, it was so large it completely filled the waveguide and reflected considerable amounts of power. The crystal also generated appreciable harmonic power. Because of these disadvantages, the crystal detector was used only for tuning and adjustment of the E.C.M. and was removed from the waveguide when data were being taken.

The microwave bolometer and sample dewar optics are discussed in the next chapter.

CHAPTER III

SAMPLE PREPARATION AND APPARATUS

Fabrication of the thin film dipoles is discussed and the experimental apparatus is described.

A. Thin Film Aluminum Dipoles

Figure 9 shows the thin film geometry used. Initially we tried several geometries with resistive dc leads at the ends of a dipole strip. This geometry proved unworkable, since the attached leads strongly affected the microwave response, unless they were made so highly resistive that heating effects interfered with the critical current measurements. The folded dipole avoids these problems.

Substrates were of Dow Corning 7059 glass and were scrubbed with detergent, rinsed in distilled water and vapor degreased in ethanol before film evaporation.

An oxide layer forms on aluminum films through which electrical contact is difficult. Evaporation of aluminum on top of nichrome contact tabs circumvented this problem and gave good electrical connection. The nichrome tabs were evaporated thin films of about 200 Ω/square resistance. Leads were indium soldered to the nichrome, which forms a tough, strongly adherent film and is not damaged by the soldering process.

An initial attempt to use gold rather than nichrome

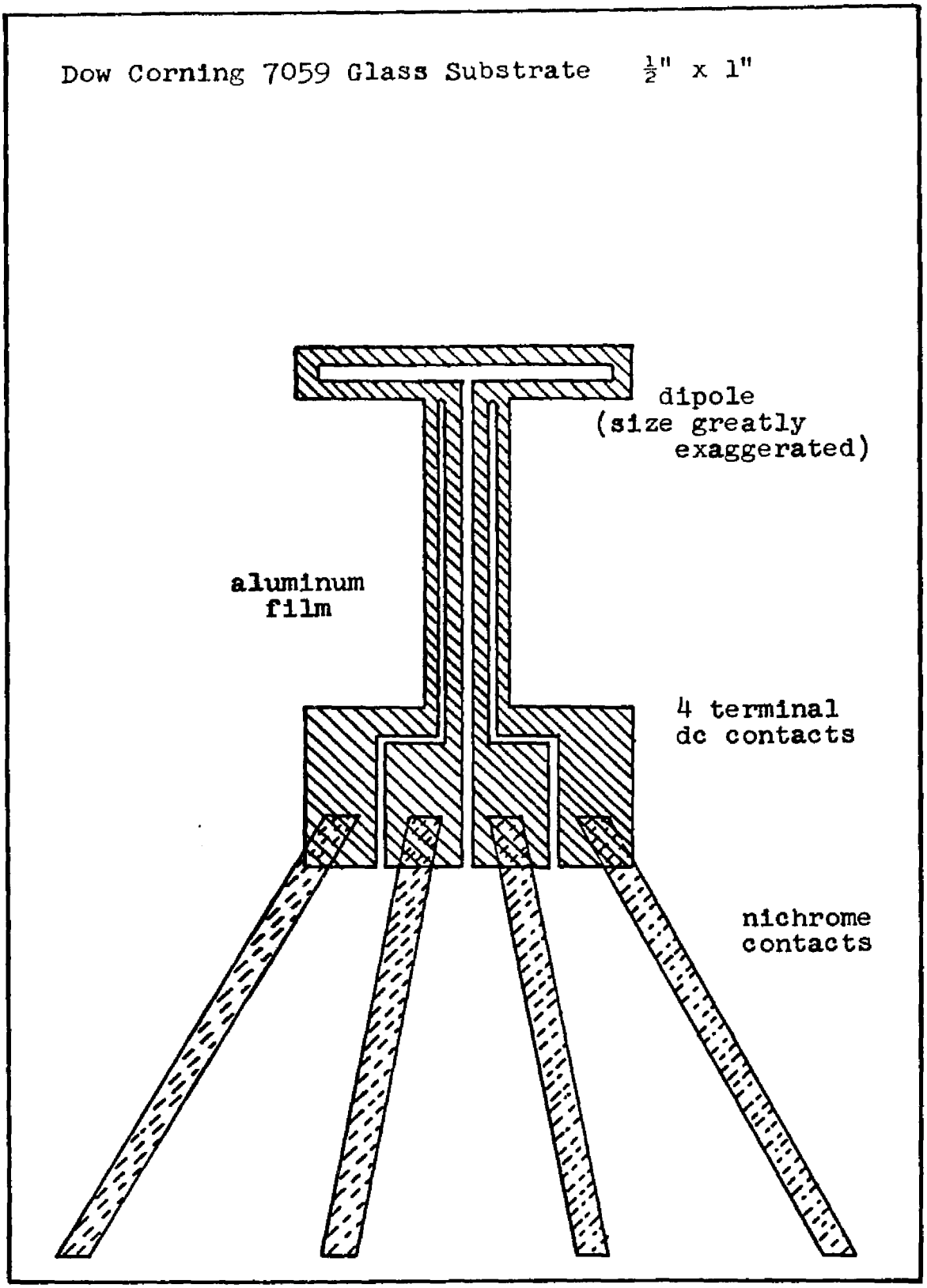

Figure 9. Thin film sample geometry.

contact tabs was unsuccessful. Aluminum films thinner than 50Å oxidized all the way through when deposited on top of gold. Usually aluminum films form an oxide layer no thicker than 20Å. Apparently the gold promotes diffusion of oxygen into the aluminum film.

The aluminum films were deposited at pressures less than 6×10^{-6} Torr and at rates greater than 20Å/sec.

Film thickness was controlled by evaporating a known weight of aluminum. The procedure was to evaporate a 6 mg charge of 99.999% pure aluminum from a tantalum boat. Some of the aluminum, typically 30%, would alloy with the tantalum and not be vaporized. The exact amount evaporated was determined by weighing boat and charge before and after the evaporation. The distribution of vapor from a dimpled boat source is experimentally known[14] and the film thickness d is given by

$$d = m/(\pi \rho r^2) \qquad \text{(III-1)}$$

where m is the mass evaporated, ρ is the density of the material, and r is the distance from boat to substrate.

The actual thickness of metal film is less than the above because of oxide formation. Holland[15] claims that freshly evaporated aluminum films rapidly oxidized to a depth of 20Å upon exposure to air. Thereafter oxidation proceeds slowly, over a period of months, to a depth of 45Å. All samples were used within a few days of film evaporation.

Making the indicated correction, we take

$$d = m/(\pi\rho r^2) - 20\text{Å} \pm 5\text{Å} \qquad \text{(III-2)}$$

to be the metal film thickness.

The dipole microgeometries were produced by scribing the aluminum films. The scribing tool was a piece broken from a Gillette Blue Blade. The tool was placed in a spring-loaded holder which held it with constant pressure against the substrate. The substrate was moved under the tool with a micromanipulator. The process was observed with an optical microscope. The tool removed a 10-20μ swath of metal film. The geometry shown in Figure 10 could be produced with an edge roughness of less than 0.5μ, as determined by optical microscope.

B. Sample Dewar

The aluminum dipoles and the microwave bolometer were placed in a 3" glass dewar.

Liquid helium vapor pressure was controlled with a 14 cfm pump and a diaphragm manostat. Temperature was measured with a carbon composition resistance thermometer, calibrated against vapor pressure.

An annealed permalloy shield was placed around the dewar, reducing the magnetic field at the region of the sample to less than 10^{-3} gauss. On the order of one gauss would be required to produce circular vortices in the dipole strip,

since it is so narrow.

To prevent spurious signals and rf induced currents, the dipole sample, bolometer, and leads were completely enclosed by metal shielding within the dewar. This shielding was insufficient since turning on the 20 kV supply for the E.C.M. caused erratic fluctuations in the dipole critical current. The problem was apparently vhf currents induced in the dipole by radiation from corona within the hv supply. A second shield was made by enclosing the entire dewar in an aluminum box. This eliminated observable noise.

In Figure 10 a cross section of the sample end of the dewar insert is shown. The major experimental problem in this piece of apparatus is to insure that, for all frequencies, the microwave power level at the superconducting dipole is the same as the power level measured by the bolometer.

To eliminate the effect of standing waves within the film substrate, the dipole side of the substrate was placed facing the bolometer. Since the electric field is tangential and thus continuous across the substrate-helium surface, the power incident upon the dipole is the same as the power incident upon the bolometer so long as there is no reflected wave from the bolometer. The bolometer, described in the next section, was designed for low reflection, but as a further precaution absorbing material was placed as shown in Figure 10 to attenuate any microwave reflection from the bolometer.

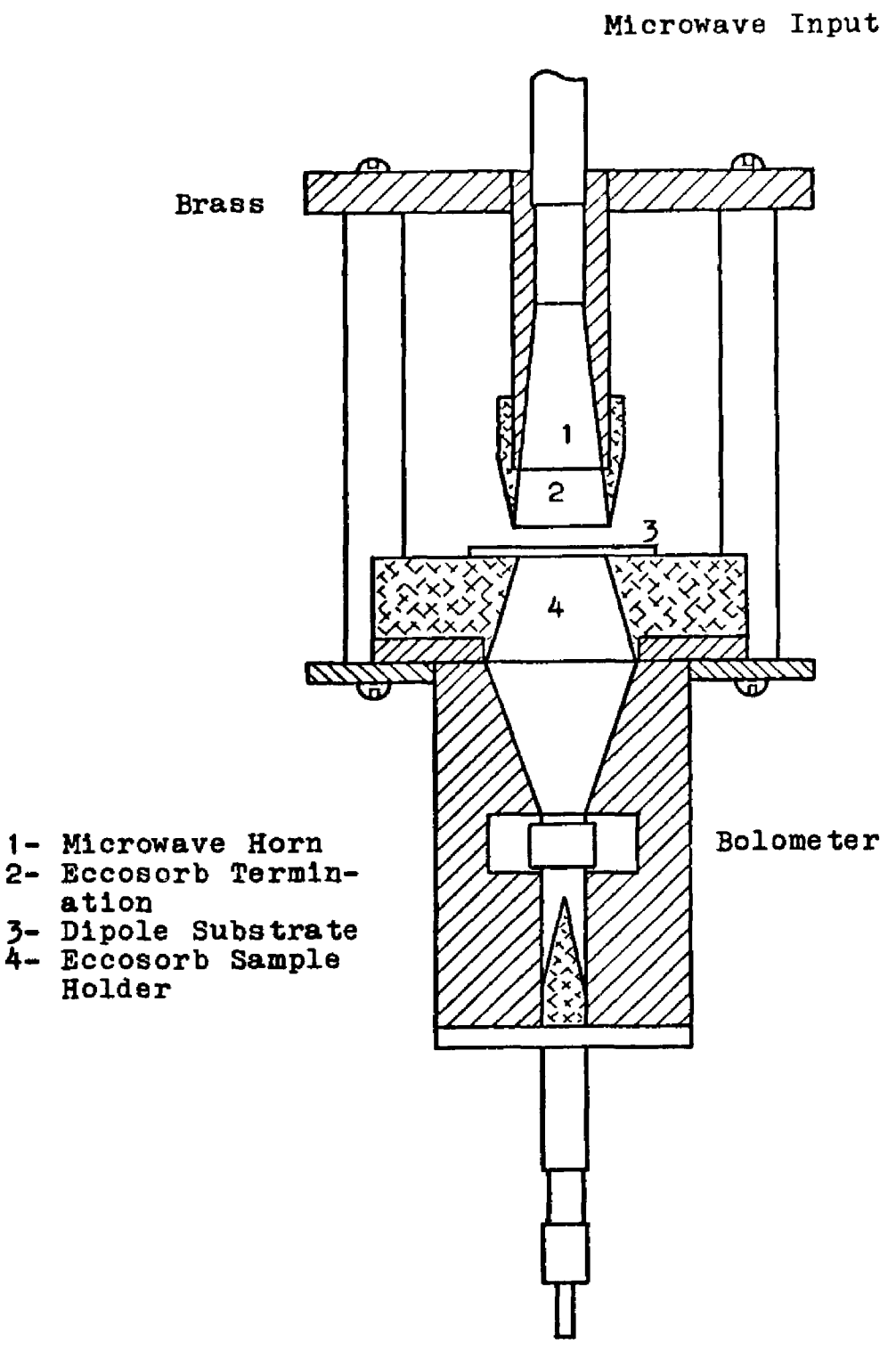

Figure 10. Sample dewar insert. The Eccosorb substrate holder is used to attenuate any reflected wave from the bolometer.

C. The Bolometer

Figure 11 shows a cross section of the microwave bolometer.

The bolometer is similar to those described by Low[16] and by Richards.[17] The active element is a single crystal of germanium, mounted in an evacuated container.

Germanium, suitably doped, provides a large temperature coefficient of resistance, high thermal conductivity, and a small heat capacity at cryogenic temperatures. These characteristics enabled construction of a highly sensitive bolometer with a rapid response time.

The germanium crystal was grown by the Chemical and Metallurgical Division of Sylvania Electric Products Inc. It was heavily doped and compensated, 2×10^{17} atoms/cc indium and 10^{17} atoms/cc antimony, to produce a large temperature coefficient of resistance at the temperatures used, 1.4-2.2°K.

The crystal, 3/8" x 1/4" x 0.020", was mounted transversely across a section of waveguide. Both ends of the crystal were heat sunk to the brass housing with four 1 mm lengths of 0.020" copper wire. The wire was indium soldered to the germanium.

The thermal relaxation time, essentially the same as the bolometer response time, was less than 100 μsec at liquid helium temperatures.

The resistance of the germanium crystal for temperatures less than 2°K was on the order of $10^6 \Omega$. With such a high impedance, the germanium would absorb very little of any

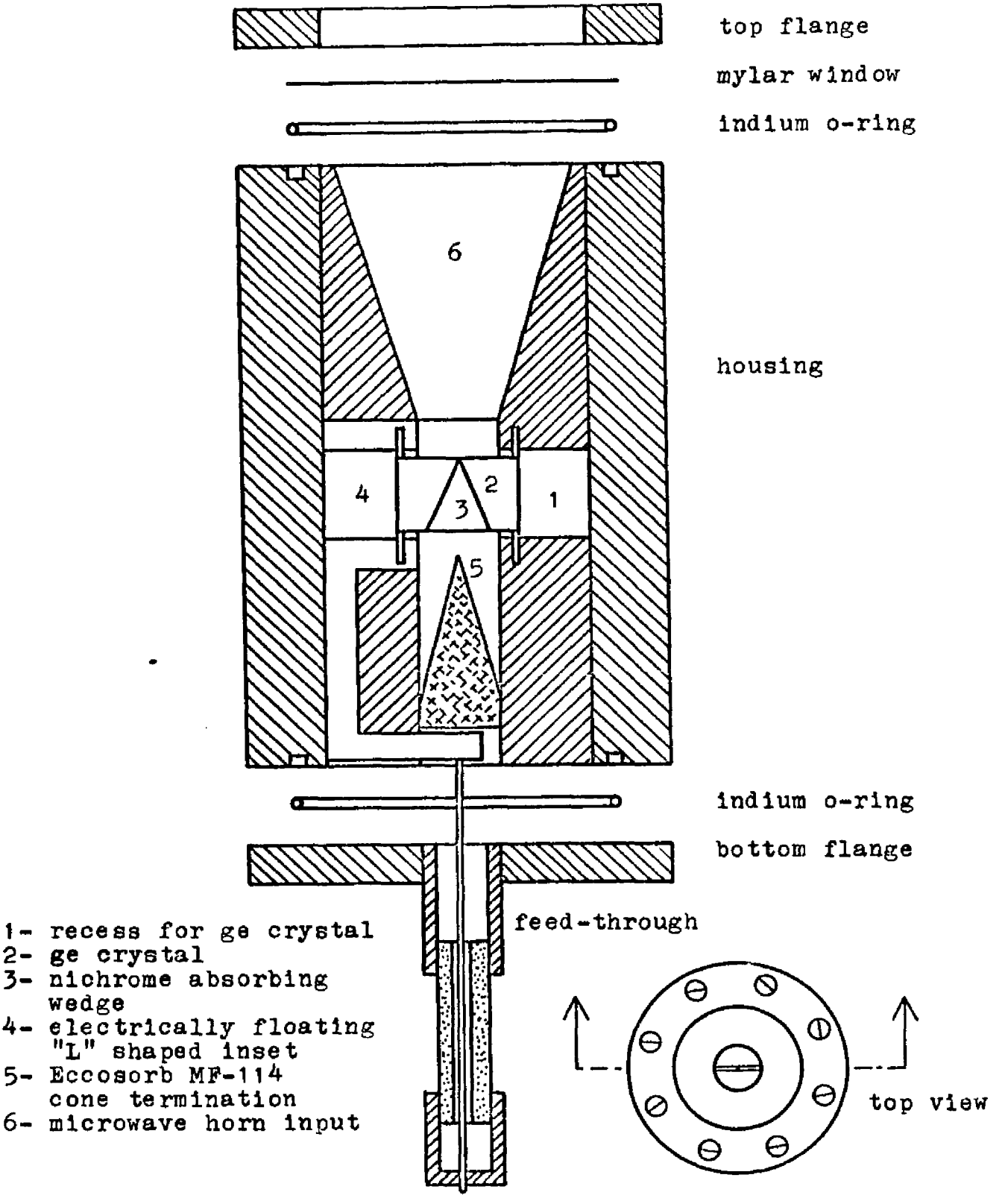

Figure 11. Cross section of microwave bolometer. Shown twice actual size.

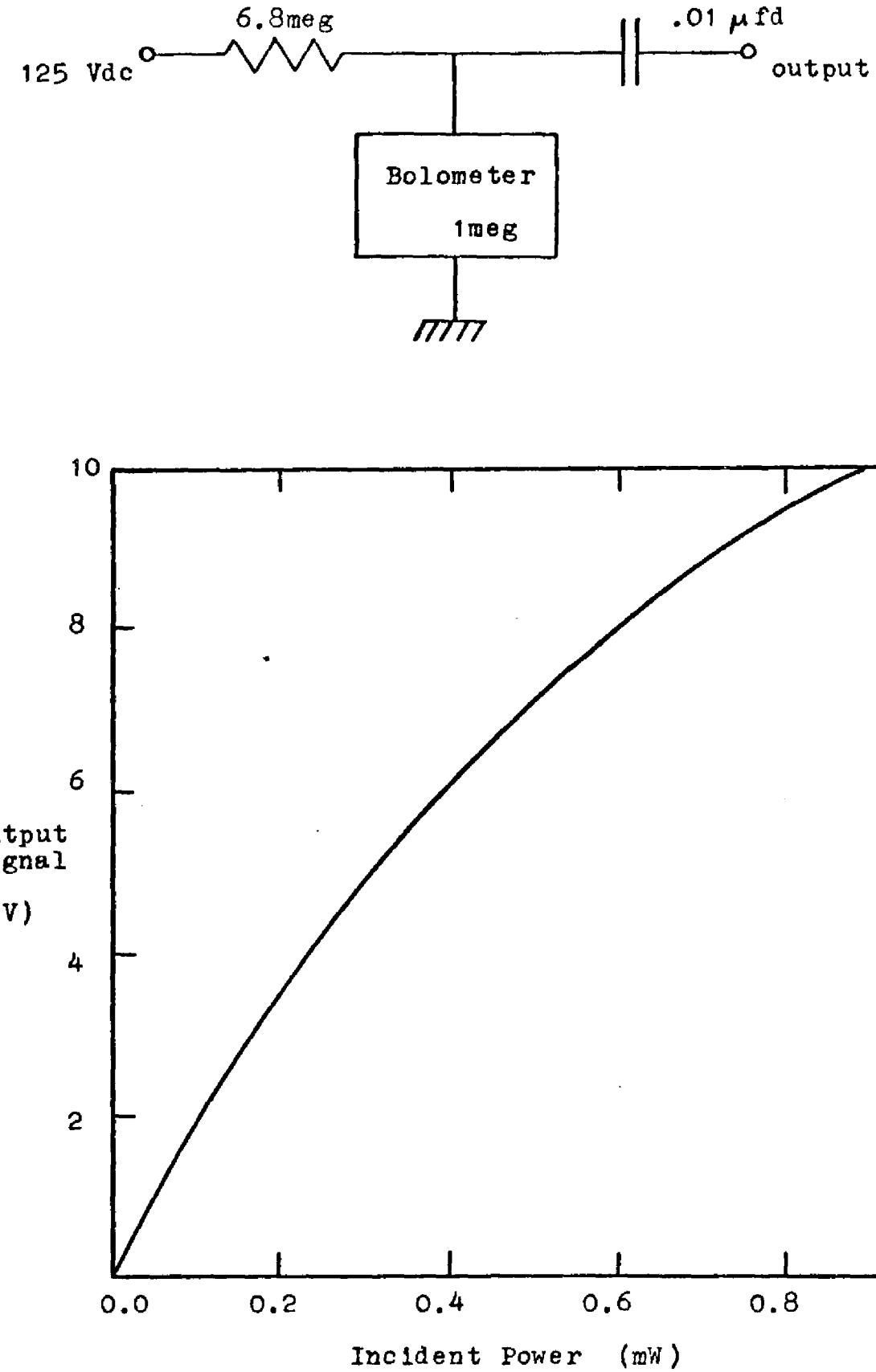

Figure 12. Bolometer circuit and response. The response was measured at a He bath temperature of 1.45 ^{o}K.

microwave power in the guide. A 100 Ω/square nichrome film was evaporated onto the germanium to form an absorbing wedge. Tests of a similar wedge indicated that it absorbs 60-90% of incident microwave power over the frequency range used.

To prevent standing wave effects from any microwave power not absorbed by the germanium crystal, an absorbing cone of Eccosorb MF-114 was used to terminate the bolometer waveguide.

By measuring the current-voltage characteristic for various helium bath temperatures, bolometer resistance as a function of input power was obtained, providing a direct calibration.

Figure 12 shows the bolometer circuit and the response calibration.

D. Electronics

Figure 13 shows the arrangement used to measure the dipole I-V curve and the incident microwave power.

A Tektronix Type 504 dual-beam oscilloscope was used to display the data. The sweep was triggered at the beginning of a microwave pulse. The sawtooth sweep waveform from the oscilloscope was amplified and used to sweep the current through the superconducting dipole, so that the upper trace displayed the I-V characteristic of the dipole while the lower trace displayed the bolometer output, measuring the incident microwave power.

Typical data is shown in the next section.

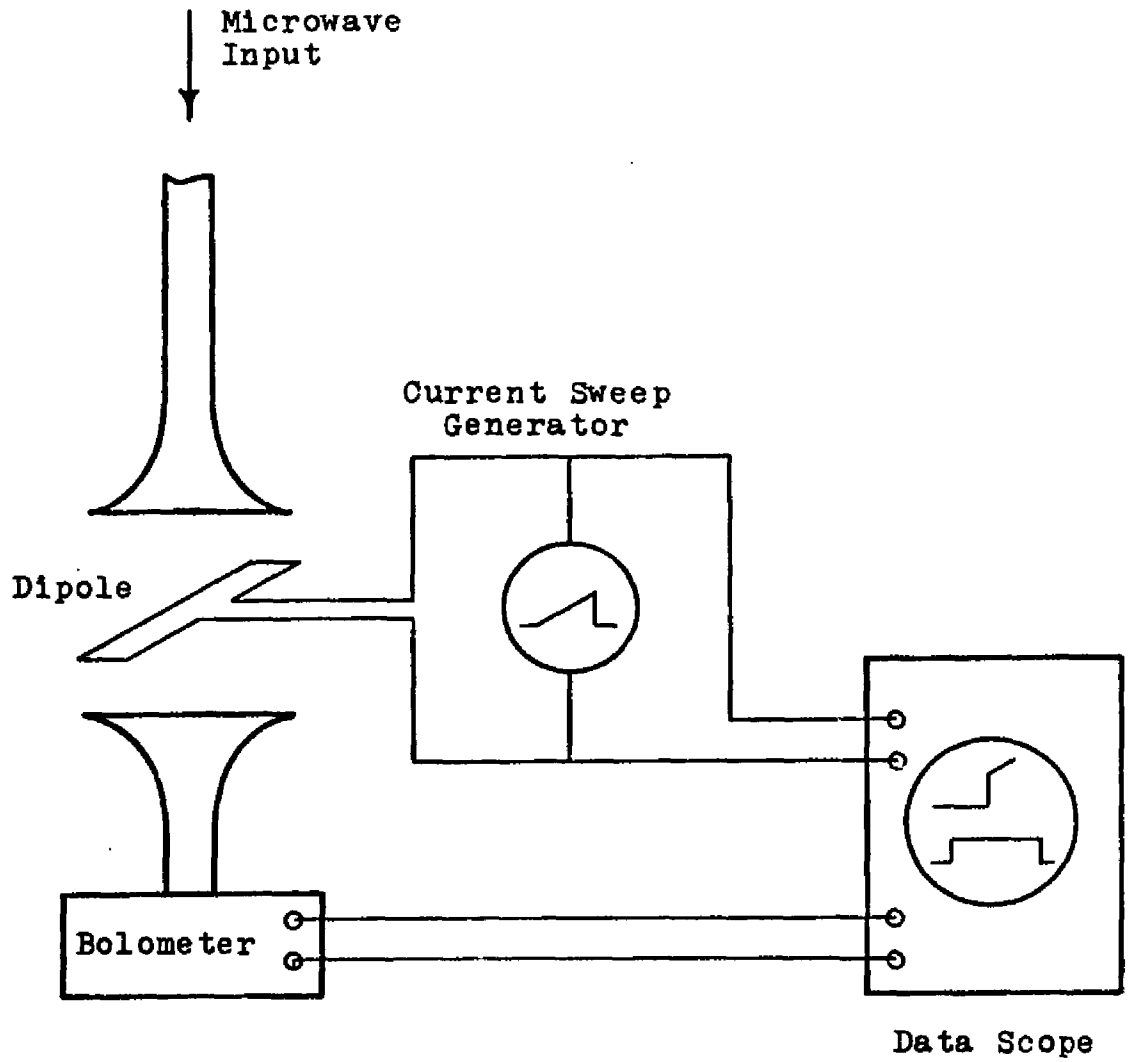

Figure 13. The experimental set-up.

CHAPTER IV

RESULTS AND DISCUSSION

We discuss the data taken, the dc behavior of the superconducting films, and the dipole resonant microwave response. Microwave enhanced critical currents are described and a model proposed.

A. Features of the I-V Curves

In Figure 14a a typical I-V curve is shown. The critical current was well defined. At currents less than the critical current, less than 1 part in 10^4 of the dipole strip was in the normal state. The slight structure in the curve of 15a indicates that the three arms of the dipole, being of slightly different widths, have small variations in critical current. At temperatures near T_c, where the critical current was small, $<10\mu A$, additional structure was observed, reflecting small variations in the width of the dipole strip and a consequent spread in critical current. For critical currents greater than $10\mu A$, joule heating in any normal region along the strip would cause propagation of the normal region at a velocity greater than $10^2 m/sec$. Because of this effect the measured critical currents correspond to the critical current of the narrowest portion of the strip.

In Figure 14b the upper trace records a family of I-V curves for varying microwave power. The lower trace is the

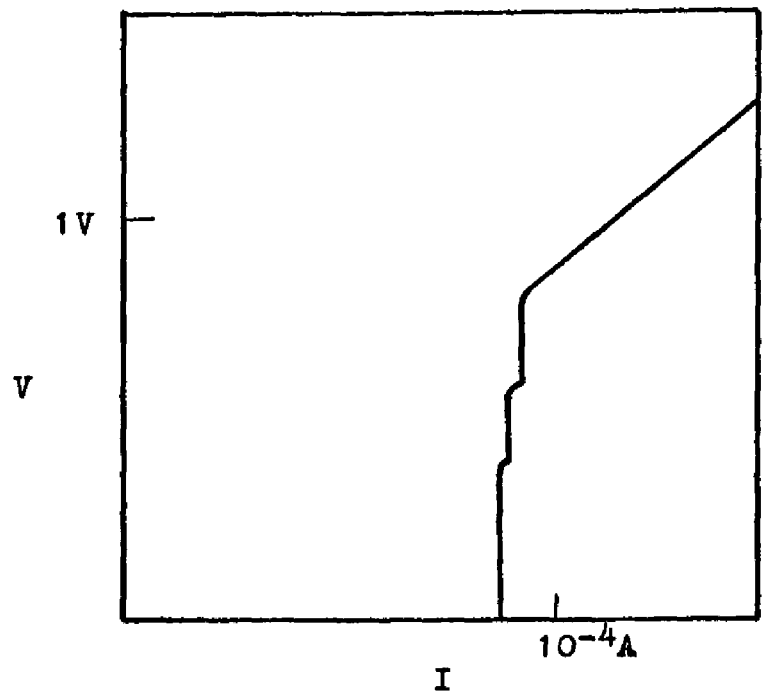

Figure 14a. Typical dipole I-V curve with no microwave field.

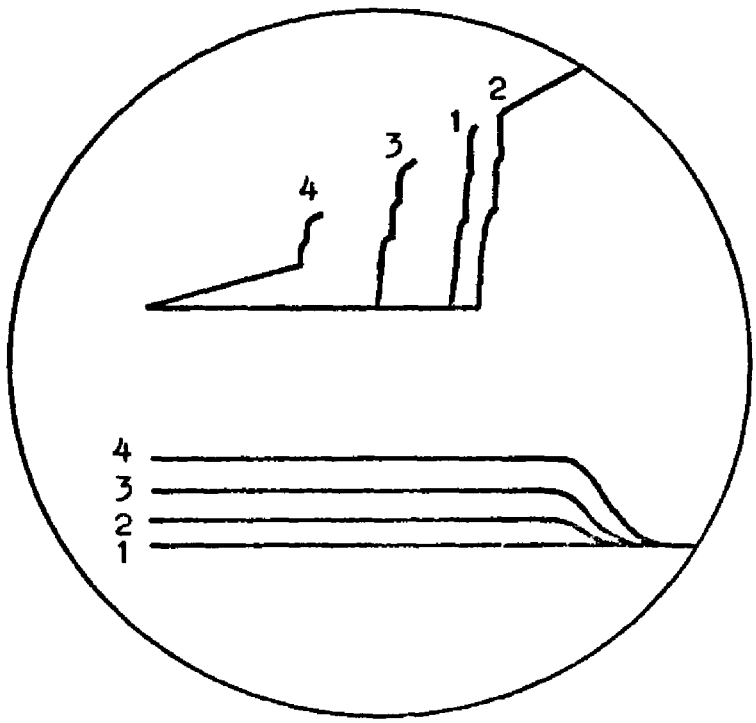

Figure 14b. Representation of oscilloscope display of a family of dipole I-V curves for varying microwave powers. The lower trace displays the bolometer output.

bolometer output, indicating the microwave power. Microwave induced structure in the I-V curve was not observed. The only effect of the microwaves was to shift the dc critical current, sometimes increasing it, as is shown in Figure 14b. With increasing microwave power, the dc critical current in one or more arms of the dipole would eventually be driven to zero.

Notice that at the highest microwave power one-half the total strip length is driven completely normal; this is taken as an indication that the microwave current is greatest in arm 1 of the dipole (see Figure 9). At higher frequencies it was sometimes observed that only one-quarter of the strip was driven normal. This information was useful in inferring the mode of microwave excitation of the dipole.

B. dc Behavior of the Superconducting Films

1. The Resistive Transition

The transition temperatures of the films studied ranged from 1.5 - 2.3°K for film thicknesses from 20 - 100Å. The transition temperature increased with decreasing film thickness. This effect is believed to be due to the phonon spectrum in thin films being different from that of bulk aluminum because of surface effects.[18,19]

Figure 15 shows a typical resistive transition. The transition widths were on the order of 30m°K. Since the transition temperature varies typically 300m°K with a 10Å change in film thickness and also varies with film structure,[18]

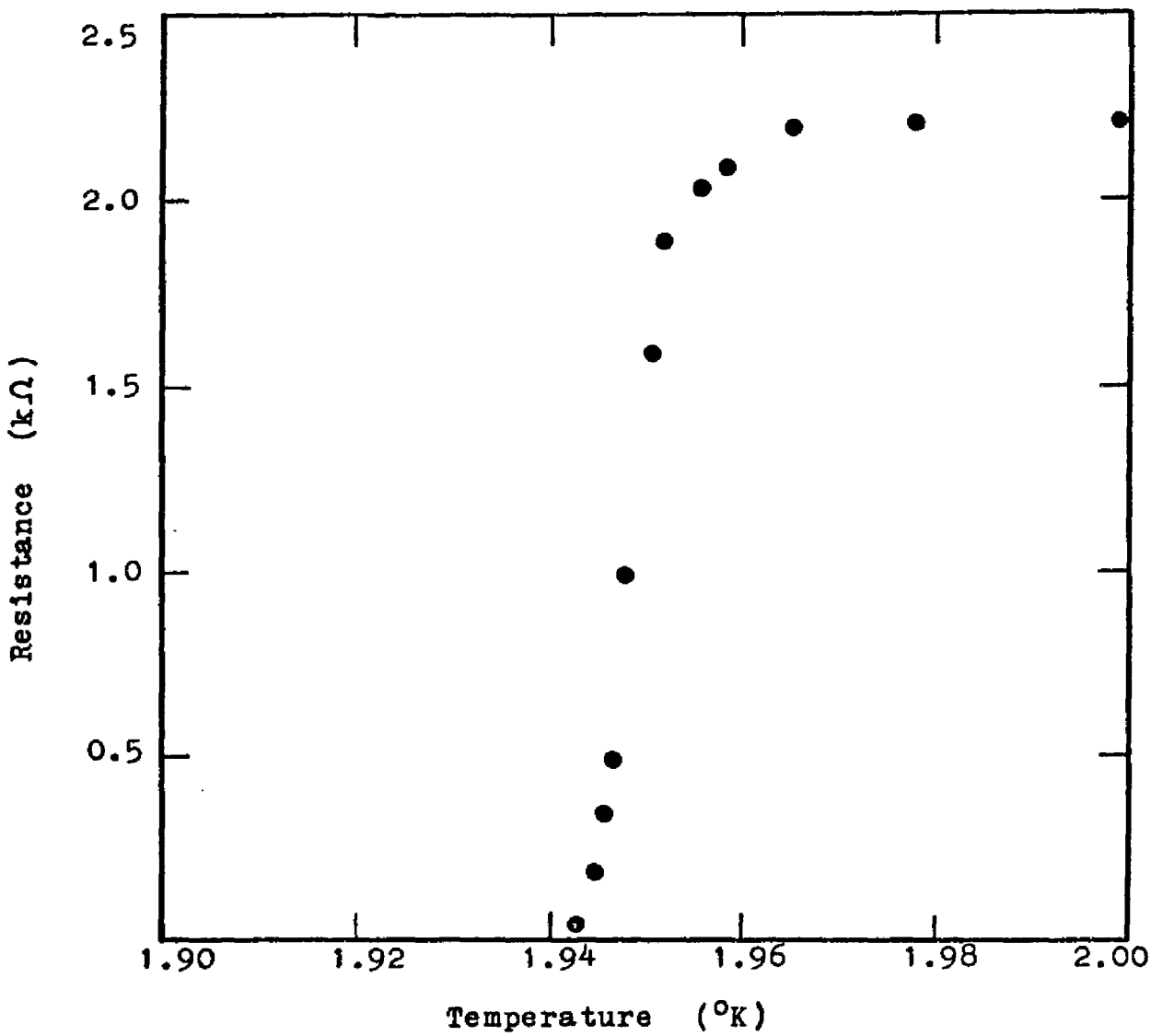

Figure 15. Typical resistive transition.

the relatively narrow transition width indicates that the films were uniform in thickness and structure.

2. Theoretical Penetration Depth

The distribution of supercurrents in the thin film strips, the critical current, and the microwave response all depend on the superconducting penetration depth λ in the thin films, which differs from the penetration depth in bulk aluminum for several reasons.

Electron scattering from the film boundaries reduces the effective coherence length and increases the penetration depth. Douglass[20] has calculated this effect and obtained, in the limit $\xi_0/d >> 1$,

$$\lambda = 0.82\lambda_{bulk}(\xi_0/d)^{\frac{1}{2}} \qquad \text{(IV-1)}$$

where ξ_0 is the bulk coherence length and d the film thickness.

Aluminum is a uniquely suitable material for this experiment because of its long coherence length and the very thin continuous films which it forms. For the films studied typically

$$(\xi_0/d)^{\frac{1}{2}} \cong (16{,}000\text{Å}/40\text{Å})^{\frac{1}{2}} = 20 \qquad \text{(IV-2)}$$

so that we expect λ_{film} to be considerably greater than λ_{bulk}. A large penetration depth is advantageous since the allowable cross sectional area A of the dipole strips scales as λ^2. As

was pointed out in Section IA, we must have $\lambda^2/A > 1$ both to insure uniform distribution of supercurrents and to provide a dominant kinetic inductance term in the microwave impedance.

Equation IV-1 is not directly applicable to thin aluminum films because of additional effects of the changed phonon spectrum.

In thin superconducting films, the penetration depth can be directly related to the normal state conductivity. Glover and Tinkham[21] verified a general relationship between the normal state conductivity σ_n and the ac diamagnetic conductivity $i\sigma_2$ of a thin film in the superconducting state,

$$\sigma_2/\sigma_n = \alpha k T_c/\hbar\omega \qquad \text{(IV-3)}$$

where k is the Boltzman constant and σ_2 the imaginary conductivity of the superconducting film at T = 0. Equation IV-3 can be obtained from the B.C.S. theory[22,23] which predicts $\alpha = 5.5$. We use the value $\alpha = 3.7$, obtained experimentally by Glover and Tinkham for a variety of films of different metals.

To relate IV-3 to the penetration depth, we consider the accelerative London equation

$$E = \mu_0 \lambda_0^2 \, i\omega J \qquad \text{(IV-4)}$$

where we assume T = 0 and an $\exp(i\omega t)$ time dependence. The imaginary conductivity σ_2 is defined by

$$J = -i\sigma_2 E \ . \qquad \text{(IV-5)}$$

Substituting into IV-4 gives

$$\sigma_2 = (\omega\mu_0\lambda_0^2)^{-1} \ . \qquad \text{(IV-6)}$$

Substituting into IV-3, we obtain

$$\lambda_0^2 = (\hbar/\alpha\mu_0)(\sigma_n k T_c)^{-1} \ , \qquad \text{(IV-7)}$$

the desired result, giving the T = 0 penetration depth in terms of two easily measured film parameters, the normal state conductivity σ_n and the transition temperature T_c. IV-7 is a general relationship, holding for any superconducting film of thickness $d << \lambda$.

To obtain $\lambda(\tau)$, we assume the usual temperature dependence

$$\lambda(\tau) = \lambda_0(1-\tau^4)^{-\frac{1}{2}} \qquad \text{(IV-8)}$$

where τ is the reduced temperature.

Both the measured critical currents and the microwave response are in good agreement with the values for λ given by IV-7 and IV-8.

3. The dc Critical Current

Glover and Coffey[24] give an expression for the current density J at the edge of a thin, flat superconducting strip as

$$J = J_0 - (d/b\lambda^2)x \qquad \text{(IV-9)}$$

where x is the distance from the edge of the strip, b is a constant of order unity, and the film thickness d is much less than λ. The supercurrent density will be uniform across the width w of the dipole strip in the limit

$$(d/b\lambda^2)w \cong A/\lambda^2 << 1 \ . \qquad \text{(IV-10)}$$

For the dipole strips studied, $A/\lambda^2 \leq 0.3$, and the supercurrent density should vary less than 15% across the width of the strip. We can reasonably assume the critical current density J_c to be given by

$$J_c = I_c/A \qquad \text{(IV-11)}$$

where I_c is the measured critical current.

Bardeen[25] calculated the critical current density for a thin superconducting film in the limit that the film thickness is much less than the bulk coherence length, with the result

$$J_c(\tau) = 2/3 \ \frac{H_0}{\lambda_0} \ (1-\tau^2)^{3/2} \qquad \text{(IV-12)}$$

where H_0 is the critical field at T = 0. This result, obtained from the B.C.S. theory, is equivalent to that obtained from the Landau-Ginsburg theory[26] near T_c. The critical current is reached when the drift velocity of the superelectrons

becomes sufficiently great that their kinetic energy exceeds the condensation energy.

In order to apply IV-12 we note that the higher transition temperatures of thin aluminum films indicate a larger condensation energy than in bulk material. We take H_0 to be an effective critical field

$$H_0 = (T_c/T_{c(bulk)})H_{0(bulk)} \qquad \text{(IV-13)}$$

since from the B.C.S. theory we expect the critical field to scale with the transition temperature.[27]

Using IV-13, and substituting IV-7 into IV-12 we obtain

$$J_c(\tau) = 2/3 \frac{H_{0(bulk)}}{T_{c(bulk)}} (\alpha \mu_0 k/\hbar)^{\frac{1}{2}} \sigma_n^{\frac{1}{2}} T_c^{3/2} (1-\tau^2)^{3/2} \qquad \text{(IV-14)}$$

for the temperature dependent critical current density of a thin film aluminum strip.

Figure 16 is a plot of measured critical current vs. temperature for four representative samples. Notice that this is a parameter-free fit. The excellent agreement with the B.C.S. predicted critical current indicates that the measured critical current is a result of depairing.

Since we will attempt to explain the microwave enhanced critical currents in terms of a modified Landau-Ginsburg free-energy it is encouraging that in the absence of microwaves the observed sample behavior can be realistically described by the Landau-Ginsburg theory.

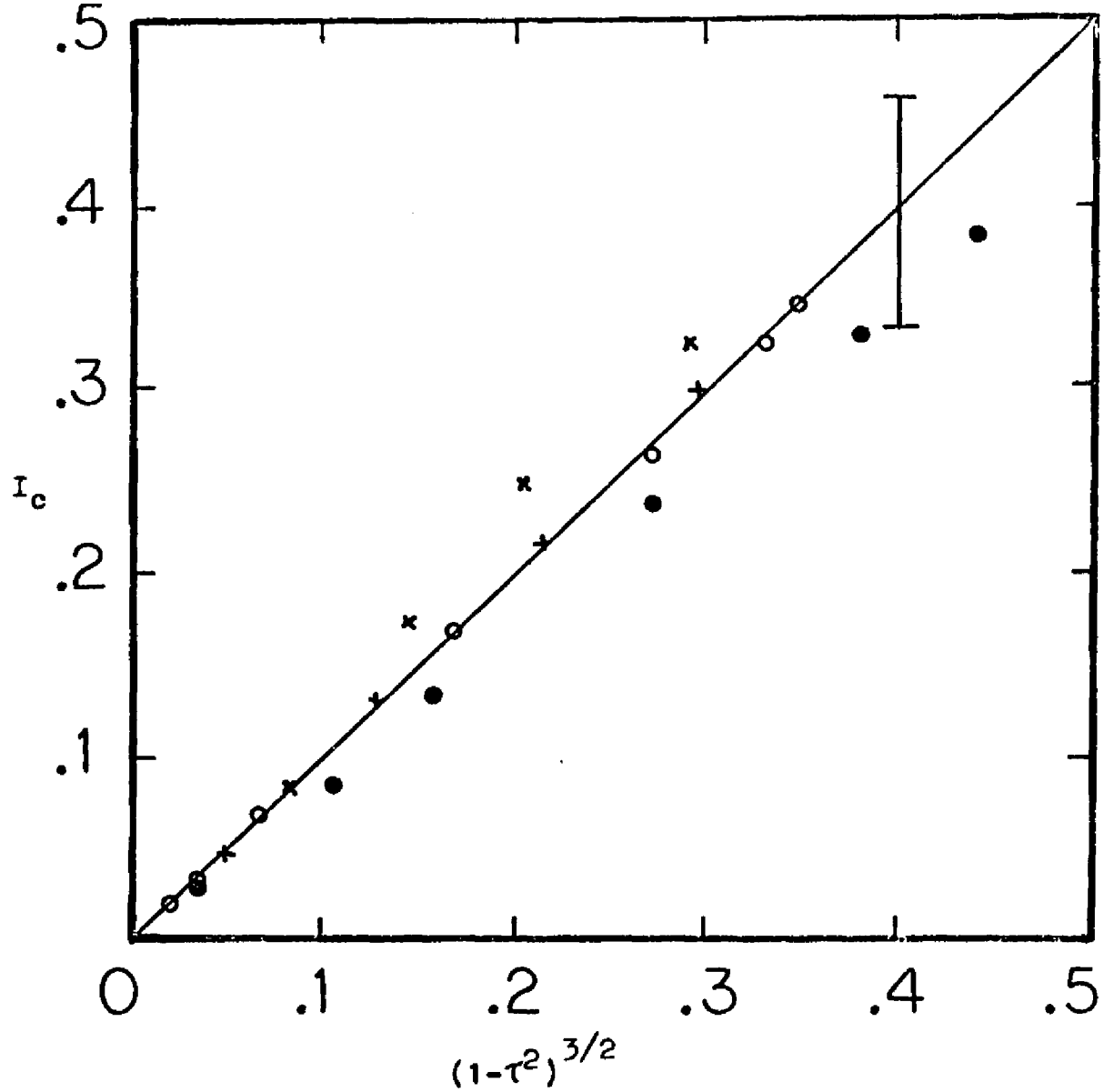

Figure 16. dc Critical Current vs. Temperature. The measured critical current is plotted in units of the predicted critical current at T=0.

C. The Microwave Response of the Dipoles

In Sections 1 and 2 we develop a model for the microwave response. In Section 3 we compare the observed response with the model.

1. Theoretical Response--The Half-wave Line

To obtain the microwave response of the folded dipole we treat it as a single strip describable by the lumped parameters of inductance L, capacitance C, and series resistance R per unit length. In fact the folded dipole consists of two superconducting lines. Arms 2 and 3 of the dipole are effectively continuous through the large capacitance of the dc leads. The upper and lower lines are coupled only at the ends and we approximate the response by ignoring the coupling and treating each line separately.

The model used is schematized in Figure 17. When a microwave field $E_0 e^{i\omega t}$ is applied parallel to the strip, the equation of motion is

$$L\frac{\partial I}{\partial t} + C^{-1}\frac{\partial q}{\partial z} + IR = E_0 e^{i\omega t} \qquad \text{(IV-15)}$$

where $I(Z,t)$ is the microwave current and $q(Z,t)$ the charge per unit length along the strip.

If we define $Q(Z)$ to be the total charge over the interval $(0,\ell)$, then

$$I = \frac{\partial Q}{\partial t}, \qquad q = -\frac{\partial Q}{\partial Z} \qquad \text{(IV-16)}$$

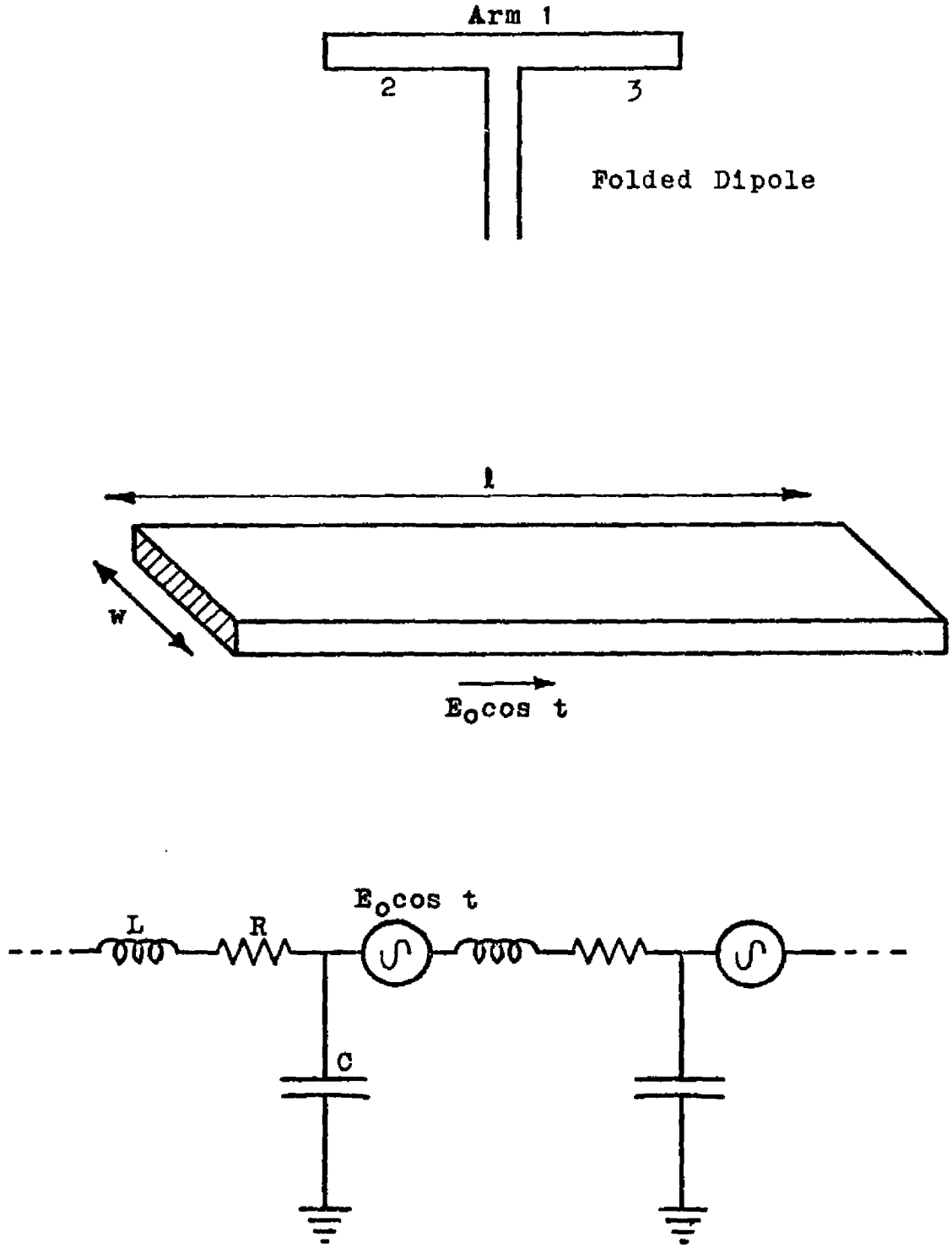

Figure 17. Transmission line model for dipole microwave response.

and IV-15 becomes

$$L\frac{\partial^2 Q}{\partial t^2} - C^{-1}\frac{\partial^2 Q}{\partial Z^2} + R\frac{\partial Q}{\partial t} = E_0 e^{i\omega t} \qquad \text{(IV-17)}$$

with boundary conditions $Q(0) = Q(\ell) = 0$.

Solving IV-16 gives

$$Q(Z,t) = \sum_{m_{odd}} Q_m \sin(m\pi Z/\ell) e^{i\omega t} \qquad \text{(IV-18)}$$

where

$$Q_m = \frac{4E_0}{m\pi L}\frac{1}{(\omega_m^2 - \omega^2) + i\omega R/L} \qquad \text{(IV-19)}$$

and

$$\omega_m = (m\pi/\ell)(LC)^{-\frac{1}{2}} . \qquad \text{(IV-20)}$$

The microwave response is a series of resonances of which we are concerned with only the lowest frequency, $m = 1$, half-wave resonance and take

$$Q(Z,t) = \frac{4E_0}{\pi L}\frac{\sin(\pi Z/\ell)\cos\omega t}{[(\omega_1^2 - \omega^2)^2 + \omega^2 R^2/L^2]^{\frac{1}{2}}} \qquad \text{(IV-21)}$$

where we have taken $\omega t \rightarrow \omega t + \theta$ in order to drop terms in the phase difference between the response and the applied field.

From IV-16 the charge and current densities induced in

the dipole strip are

$$q(Z,t) = \frac{-4E_0}{\ell L} \frac{\cos(\pi Z/\ell)\cos\omega t}{[(\omega_1^2-\omega^2)^2 + \omega^2 R^2/L^2]^{\frac{1}{2}}} \qquad \text{(IV-22)}$$

and

$$I(Z,t) = \frac{-4E_0}{\pi L} \frac{\sin(\pi Z/\ell)\sin\omega t}{[(\omega_1^2-\omega^2)^2 + \omega^2 R^2/L^2]^{\frac{1}{2}}} \; . \qquad \text{(IV-23)}$$

The resonant frequency is

$$\omega_1 = (\pi/\ell)(LC)^{-\frac{1}{2}} \; . \qquad \text{(IV-24)}$$

2. The Impedance of the Superconducting Strip

Figure 18 schematizes a two-fluid model for the strip impedance, consisting of a kinetic inductance L_k of the superfluid in parallel with a resistance R_e of the excitations or normal fluid and a geometrically determined magnetic inductance L_m. We assume a Gorter-Casimir temperature dependence in which the fraction of electrons which are superconducting varies as $(1-\tau^4)$. Other workers[28] have used this crude, but physically straightforward model for the temperature dependent microwave impedance of superconducting thin films. This model ignores variation of the order parameter with microwave current and, strictly speaking, is a linear approximation valid in the limit of small currents.

The kinetic inductance is inversely proportional to the superfluid density and we take

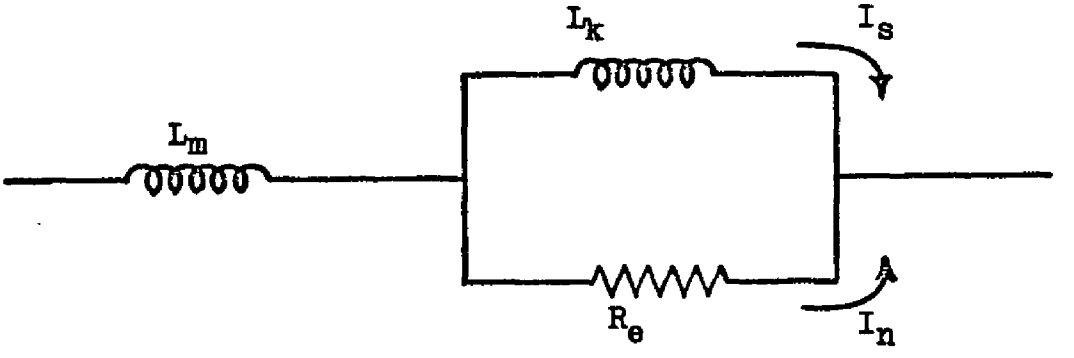

Figure18. Two fluid impedance model.

$$L_k = L_{kO}(1-\tau^4)^{-1} \qquad \text{(IV-25)}$$

where

$$L_{kO} = \mu_O \lambda_O^2 / A \qquad \text{(IV-26)}$$

is the $T = 0$ value of the kinetic inductance.

The resistance of the excitations, or normal fluid, will be inversely proportional to the fraction of electrons in the normal state and must equal the normal state resistance R_n at $T = T_c$. So we take

$$R_e = R_n \tau^{-4} \ . \qquad \text{(IV-27)}$$

The magnetic inductance L_m is given by[29]

$$L_m = 0.2(\log_e(4\ell/w)-1) \times 10^{-6} \text{ Hy/m} \ , \qquad \text{(IV-28)}$$

and depends only on the length ℓ and width w of the strip.

The lumped parameters used in the preceding section are given in terms of the known impedances L_{kO} and R_n as

$$L = L_m + \frac{L_{kO}}{(1-\tau^4)} \left[1 + \frac{\omega^2 L_{kO}^2}{R_n^2} \left(\frac{\tau^4}{1-\tau^4} \right)^2 \right]^{-1} \qquad \text{(IV-29)}$$

and

$$R = R_n \tau^{-4} \left[1 + \frac{R_n^2}{\omega^2 L_{kO}^2} \left(\frac{1-\tau^4}{\tau^4} \right)^2 \right]^{-1} \ . \qquad \text{(IV-30)}$$

Figure 19 shows the variation of effective inductance L with temperature and frequency. At low temperatures the effective inductance is nearly equal to the kinetic inductance. With increasing temperature the effective inductance increases, along with the kinetic inductance, to a maximum value characterized by $\omega L \cong \omega L_k \cong R_e$. With a further increase in temperature any rf current is predominantly a normal fluid current characterized by the resistance R_e.

The model used is not valid for frequencies greater than the temperature dependent gap frequency, in which case there are additional dissipative effects.

The capacitance C per unit length of the strip is determined by the strip geometry and the dielectric constant of the substrate material and is given by[30]

$$C = \frac{\epsilon+1}{2} \left(24/\log_{10}(2\ell/w)\right) \times 10^{-12} \text{ F/m} . \qquad \text{(IV-31)}$$

The dielectric constant of the substrate material, Dow Corning 7059 glass, was measured at audio frequencies and found to be $\epsilon = 5.5$.

When the above impedances are substituted into IV-23 we obtain the predicted temperature dependent microwave response. Qualitatively, the anticipated response is a dipole resonance, the resonant frequency decreasing with increasing temperature and the resonance being heavily damped for temperatures $\tau > 0.9$.

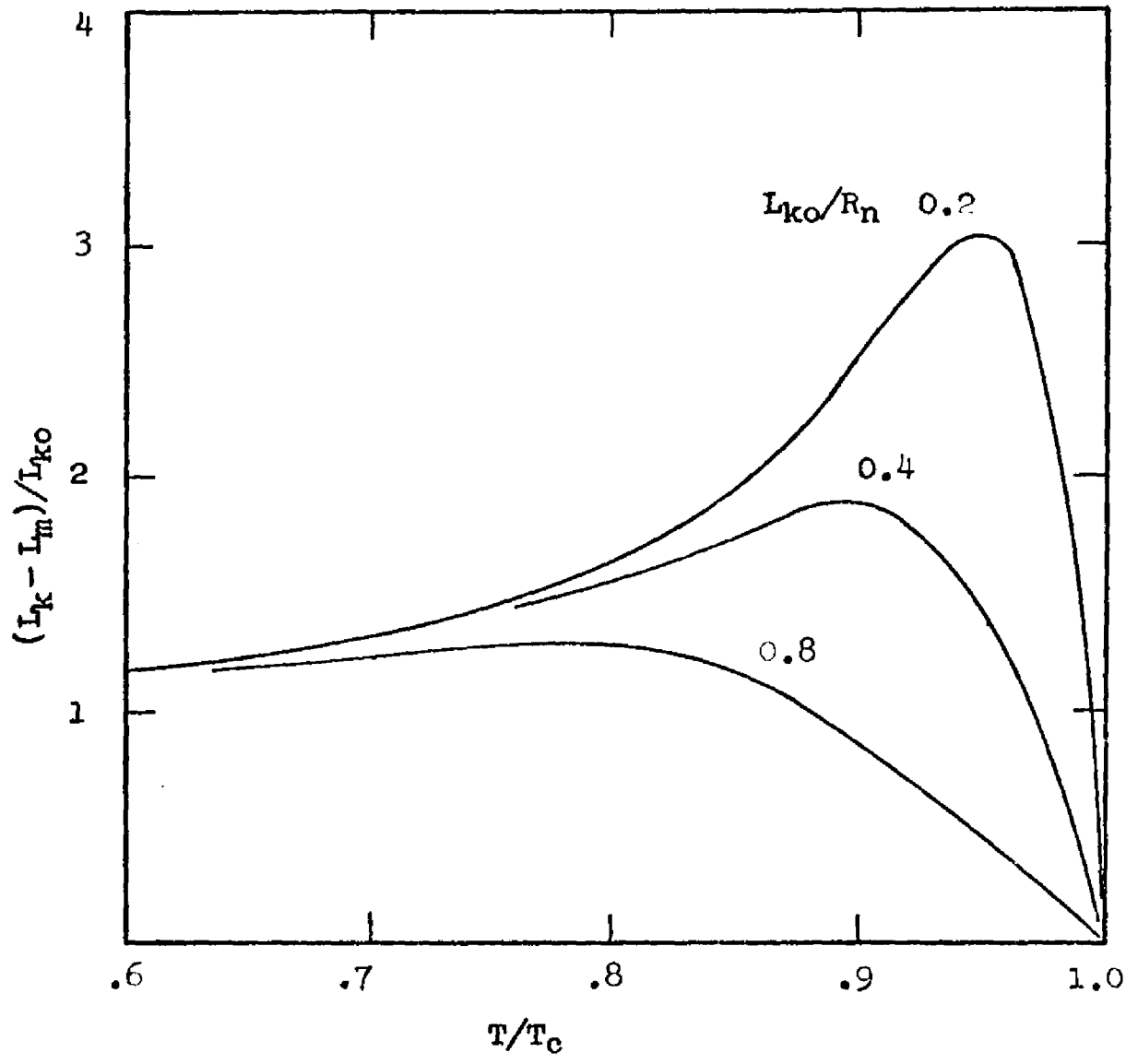

Figure 19. Effective inductance vs. temperature. The inductance plotted is the effective kinetic inductance normalized to its value at T 0.

3. The Experimental Microwave Response

The microwave response is measured by increasing the incident microwave power to a level P_c at which the dipole is driven normal, i.e. the dc critical current is reduced to zero. We assume that for incident power P_c the peak microwave current induced in the dipole is equal to I_{c_0}, the critical current in the absence of microwaves.

In Figure 20 the measured response for a typical dipole is plotted as a response function

$$R(\omega) = \frac{I_{c_0}^2}{P_c(\omega)} \left(\frac{c\epsilon_0}{2}\right) , \qquad \text{(IV-32)}$$

which is the squared ratio of microwave current to microwave field.

The solid curve is the response predicted by IV-22.

Table 1 lists predicted and observed resonant frequencies for all the dipoles studied.

The agreement of predicted and observed microwave response is remarkable considering some of the approximations made in the model.

It should be emphasized that the model contains no adjustable parameters, the microwave response being completely determined by the dipole geometry and the transition temperature and normal state resistance of the film.

The arrow in Figure 20 indicates a somewhat smaller resonance at higher frequency found in all the dipoles studied. It was invariably found that the more prominant

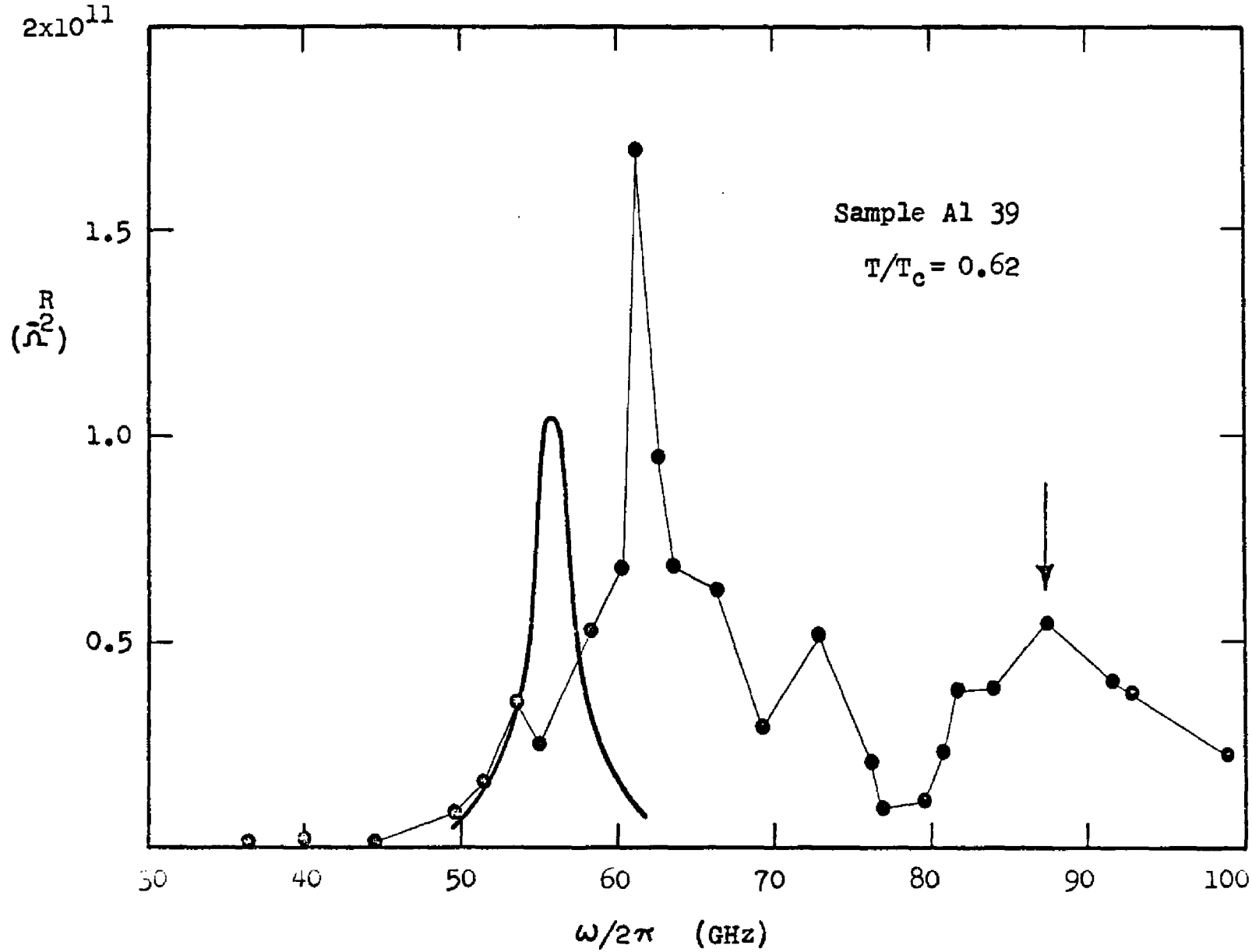

Figure 20. Dipole microwave response. The solid curve is the predicted dipole resonant response and carries an uncertainty of 30% in frequency and +100% -50% in amplitude. The arrow indicates a higher mode excitation.

Sample	Reduced Temperature	Resonant Frequency $\omega_1/2\pi$ Predicted	Observed	$\omega_{obs.}/\omega_{pred.}$
Al-39	0.62	56.6 GHz	61.5 GHz	1.09
	0.73	52.1	56.6	1.09
	0.80	48.2	52.6	1.09
Al-38	0.75	110	100	--
	0.90	overdamped	overdamped	--
Al-36	0.65	54.1	59.8	1.11
	0.78	48.2	55.5	1.15
	0.86	43.2	51.0	1.18
Al-35	0.76	51.2	56.0	1.09
	0.87	48.5	54.3	1.11

Table 1 Comparison of Observed and Predicted Resonant Frequencies in Superconducting Dipoles

The ratio of predicted and observed resonant frequencies is included to show that the observed resonant frequencies scale with temperature in accordance with the model used.

resonance at lower frequencies occurred in arm 1 of the dipole (see Fig. 10), while at the higher frequency resonance either arm 2 or 3 was driven normal. Arms 2 and 3 of the dipole constitute a line typically 20% shorter than arm 1 and would resonate at a correspondingly higher frequency in the absence of coupling. The observed response indicates that coupling between the upper and lower arms of the dipole does not greatly affect the response and can be neglected.

Since the microwave frequencies used are greater than the inverse relaxation time of the order parameter,[31] the microwave critical current may differ somewhat from the dc value. We have assumed them equal in lieu of a time-dependent theory for the high-frequency critical current. Although the observed magnitude of the microwave response shows that the high-frequency and dc critical currents are roughly the same, the data do not permit a detailed comparison.

The temperature dependence of the observed resonant frequencies confirms the impedance model used and shows that the microwave response is indeed coupled to the order parameter.

This result will be used in an attempt to explain the observed microwave induced increase in critical current described in the next section.

D. Microwave Enhanced Critical Currents

1. Introduction

Figure 21 shows the dc critical current in a dipole as a function of applied microwave power at various frequencies.

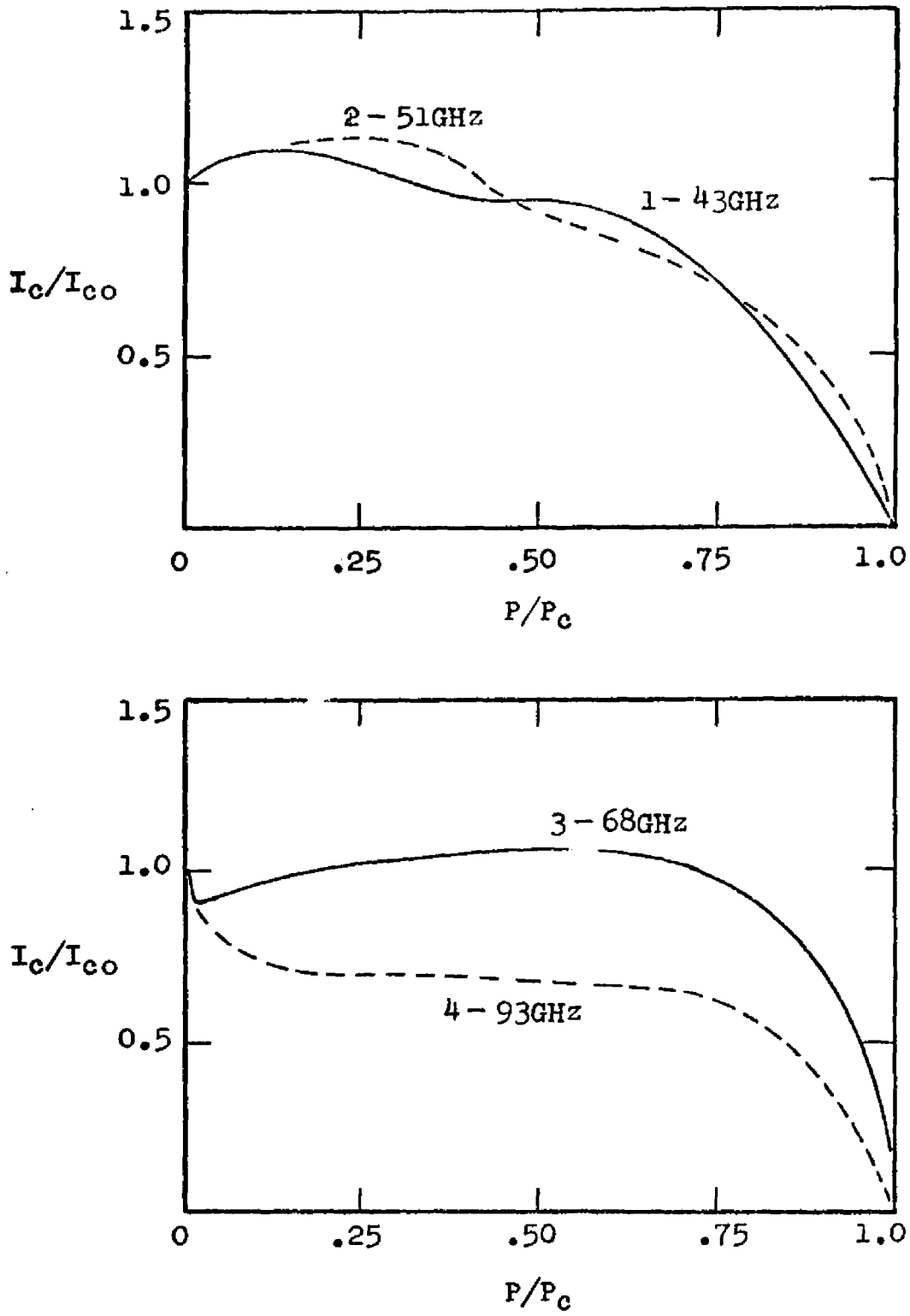

Figure 21. dc critical current vs. microwave power. Data for sample A1 36 for $T/T_c = 0.65$.

The lower frequency curves show the enhancement. A microwave induced increase in the dc critical current has been observed in nearly all the dipoles studied.

This effect was not anticipated and seems unusual, since one would expect any microwave current effectively to add to the dc current and reduce the measured dc critical current. The observed increase indicates that there is an interaction between the microwave field and the superconducting dipole which either directly increases the condensation energy of the superconductor, or causes the superconducting state to become metastable for currents larger than the critical current.

We found that a similar microwave induced increase in critical current, known as the Wyatt effect, had been observed in thin-film weak links of Sn by several investigators.[32,33] It seems probable that the present study is of the same phenomenon although the dipoles behave differently from the weak links in several respects.

Since the dipole strips vary in width, it could be argued that the narrowest spot in a dipole constitutes a weak link, and that the phenomenon observed is a weak link effect. However, we have several times observed a percentage increase in critical current more than three times as large as the percentage width variation of the dipole strip. We take this as evidence that the critical current is increased throughout the entire dipole and that the enhancement is not a localized effect.

In the next section we discuss the observed enhancement

and in the following section propose a model for the effect.

2. The Observed Phenomena

Several qualitative features of the data shown in Figure 21 were typical of the dipoles studied.

For temperatures $\tau < 0.9$, and microwave frequencies well below the dipole resonance, I_c would initially increase with increasing microwave power, pass through a maximum and go to zero, as in curve 1.

At frequencies well above the dipole resonance, no enhancement was observed, I_c decreasing monotonically with increasing microwave power, as in curve 4.

For most of the dipoles studied, there was a range of intermediate frequencies over which I_c vs P displayed a minimum, as in curve 3.

At the lowest temperatures observed, $\tau \cong 0.65$, the maximum enhancement was from 2-10%. With increasing temperature the maximum enhancement increased to 10-100% at $\tau \cong 0.9$. With further increase in temperature the enhancement rapidly disappeared.

The sample with the highest transition temperature behaved somewhat differently at the lowest temperature observed, $\tau = 0.6$, with $I_c(p)$ displaying a minimum at all frequencies below the dipole resonance. Since the present apparatus does not cool below $T = 1.45^{\circ}K$, it is not known if the other samples would have behaved similarly at the same reduced temperature.

Wiegand and Dayem[33] found no enhancement for weak link constriction widths greater than a few microns. We studied one aluminum strip sufficiently wide (18μ) that $A > \lambda^2$ and found no enhancement.

The behavior of the dipoles studied differs in several respects from earlier studies of the Wyatt effect in weak links.

In weak links measurable enhancement occurs only for temperatures near (within 50 m^{o}K) the transition temperature, the enhancement increasing as the transition is approached.

No minimum in $I_c(p)$ has been reported in the weak link studies.

Although the microwave enhancement is a complex phenomenon, and at present we have too little data to be sure of having identified all the essential features, one result of the present study suggests a simple model for the microwave enhancement of dc critical currents.

In two of the dipoles studied, for reduced temperatures $\tau < 0.75$, an abrupt change in $I_c(p)$ from the shape of curve 1 to the shape of curve 3 occurred at the dipole resonance frequency (see Figure 21).

In the other two dipoles studied, and for other temperatures, enhancement was observed for frequencies below the dipole resonance but not at frequencies well above the dipole resonance.

3. A Model for Microwave Enhanced Superconductivity

The observation of an abrupt change in the enhancement behavior at the dipole resonance frequency suggests that the enhancement is related to the dipole resonance. The model proposed for the microwave enhancement results from including in the free energy of the superconductor the energy of the dipole excitation.

A proper calculation would require a time dependent Landau-Ginsburg formalism valid at frequencies comparable to the gap frequency and including non-vanishing charge densities and dissipative effects. In lieu of such a formalism, we use the following approach. Using equations (IV-22) and (IV-23) for the microwave current and charge density we calculate the dipole excitation energy $\mathcal{E}$. For a fixed microwave field E_0 and frequency ω, $\mathcal{E}$ depends parametrically upon the order parameter $|\psi|^2$ through the kinetic inductance. Including the $|\psi|^2$ dependence explicitly, we add the time-average of $\mathcal{E}(|\psi|^2, E_0, \omega, t)$ to the free energy. Since the microwave frequencies used are larger than the inverse relaxation time of the order parameter, we assume that the order parameter minimizes a time-averaged free energy. This gives an expression for the dc critical current which depends upon the frequency and amplitude of the microwave field.

In order to simplify the discussion we will consider the case that $L_m << L_k << R_e$ and ignore resistive damping so that the microwave response is approximated by

$$\mathcal{J} = -\frac{4E_0}{\pi L_k}\,\frac{\sin(\pi Z/\ell)\,\sin\omega t}{\omega_1^2-\omega^2} \qquad \text{(IV-33)}$$

and

$$q = -\frac{4E_0}{\ell L_k}\,\frac{\cos(\pi Z/\ell)\,\cos\omega t}{\omega_1^2-\omega^2} \qquad \text{(IV-34)}$$

where we use $\mathcal{J}$ to designate the microwave current in order to distinguish the dc current I.

The self-energy of the dipole excitation is

$$\mathcal{E} = \tfrac{1}{2}L_k\mathcal{J}^2 + \tfrac{1}{2}C^{-1}q^2 \ . \qquad \text{(IV-35)}$$

Explicitly,

$$\mathcal{E} = \frac{8E_0^2}{\pi^2 L_k}\,\frac{1}{(\omega_1^2-\omega^2)^2}\left[\omega^2\sin^2(\pi Z/\ell)\sin^2\omega t + \omega_1^2\cos^2(\pi Z/\ell)\cos^2\omega t\right] \qquad \text{(IV-36)}$$

Time-averaging and using the approximation $\omega \cong \omega_1$ gives

$$\bar{\mathcal{E}} = \frac{4E_0^2}{\pi^2 L_k}\,\frac{\omega_1^2}{(\omega_1^2-\omega^2)^2} \qquad \text{(IV-37)}$$

which is valid for frequencies ω near the resonant frequency.

We want to include explicitly the dependence of the microwave response upon the order parameter. We define

$$f = \frac{|\psi|^2}{|\psi_0|^2} \qquad \text{(IV-38)}$$

where $|\psi_0|^2$ is the zero current value of the order parameter. We have previously noted that the kinetic inductance depends on the order parameter through $L_k \propto \lambda^2 \propto |\psi|^{-2}$, so we take $L_k \rightarrow f^{-2}L_k$ and $\omega_1 \rightarrow f\omega_1$ in IV-37 to obtain the desired form for the excitation energy,

$$\bar{\mathcal{E}} = \frac{4E_0^2}{\pi^2 L_k \omega_1^2} \frac{1}{(1-\frac{\omega^2}{\omega_1^2 f^2})^2} \quad . \qquad \text{(IV-39)}$$

For the thin film strips studied, the transverse dimensions are sufficiently small that we consider the order parameter constant over the cross section. We can write a Landau-Ginsburg free energy[34] per unit length as

$$F = A(\alpha|\psi|^2 + \beta/2\,|\psi|^4) + \frac{L_k}{2f^2} I^2 + \bar{\mathcal{E}} \qquad \text{(IV-40)}$$

where A is the cross sectional area and we include the microwave excitation energy. The term $\frac{1}{2}L_k I^2$ represents the kinetic energy of the dc supercurrent. We have used the fact that $L_k >> L_m$ and dropped terms in the magnetic field since the field energy $\frac{1}{2}L_m I^2 << \frac{1}{2}L_k I^2$.

Now $|\psi|^2$ minimizes F for constant fields, but we want to consider the case that I is held fixed. The desired thermodynamic potential is obtained by the Legendre transformation[34]

$$F - I\frac{\partial F}{\partial I} = G \qquad \text{(IV-41)}$$

giving

$$G = A|\psi_0|^2(\alpha f^2 + \beta/2\,|\psi_0|^2 f^4) - \frac{L_k}{2f^2} I^2$$

$$+ \frac{4E_0^2}{\pi^2 L_k \omega_1^2} \frac{1}{(1-\frac{\omega^2}{f^2\omega_1^2})^2} . \qquad \text{(IV-42)}$$

Minimizing G with respect to f^2, we obtain

$$A|\psi_0|^2(\alpha + \beta|\psi_0|^2 f^2) + \tfrac{1}{2} L_k I^2 \frac{1}{f^4}$$

$$- \frac{16E_0^2}{\pi^2 L_k \omega_1^2} \frac{\omega^2}{\omega_1^2} \frac{1}{(1-\frac{\omega^2}{f^2\omega_1^2})^3} \frac{1}{f^4} = 0 \qquad \text{(IV-43)}$$

or

$$I^2 - \frac{32E_0^2}{\pi^2 \omega_1^2 L_k^2} \frac{1}{(1-\frac{\omega^2}{f^2\omega_1^2})^3} = (\frac{2A|\psi_0|^4}{L_k}) f^4(1-f^2) \qquad \text{(IV-44)}$$

where we have used $|\psi_0|^2 = -\alpha/\beta$ and taken $\omega^2/\omega_1^2 \cong 1$.

We can set the microwave field $E_0 = 0$ in IV-44, and solve for the unperturbed dc critical current I_{co}, obtaining

$$I_{co}^2 = \frac{4}{27} (2A|\psi_0|^4/L_k) \qquad \text{(IV-45)}$$

which we use in IV-44 to obtain

$$I^2/I_{co}^2 = \frac{27}{4} f^4(1-f^2) + \frac{32}{\pi^2}(\frac{E_0}{\omega_1 L_k})^2 \frac{1}{I_{co}^2} (1-\frac{\omega^2}{f^2\omega_1^2})^{-3} . \qquad \text{(IV-46)}$$

In the limit $E_0 \rightarrow 0$ we can solve IV-46 for the dc critical current, obtaining

$$I_c^2/I_{co}^2 = 1 + \frac{32}{\pi^2} \left(\frac{E_0}{\omega_1 L_k}\right)^2 \frac{1}{I_{co}^2} \left(1-\frac{3}{2}\frac{\omega^2}{\omega_1^2}\right)^{-3} . \qquad \text{(IV-47)}$$

In this model we obtain microwave enhanced critical currents for frequencies $\omega^2 < \frac{2}{3}\omega_1^2$. The effect results from its being energetically unfavorable for the order parameter to assume values which put the dipole into resonance with the applied field. An increasing dc current decreases the order parameter, decreasing the resonant frequency of the dipole. If we apply a microwave field of frequency just below the resonant frequency, the resonance forms a free energy barrier against any decrease in the order parameter and creates a metastable state for supercurrents exceeding the critical current.

In Figure 22 the two terms on the R.H.S. of IV-46 are plotted separately. We have included a small damping term to remove the singularity at $f = \omega/\omega_1$.

In case A, $\omega < \sqrt{2/3}\,\omega_1$, an increase in the microwave field monotonically increases the dc critical current.

In case B, $\sqrt{2/3}\,\omega_1 < \omega < \omega_1$, an increasing microwave field first decreases, then increases I_c. The model gives the experimentally observed minimum in $I_c(p)$.

For case C, $\omega > \omega_1$, increasing the microwave field monotonically decreases I_c.

Comparison of IV-47 with the available data is not

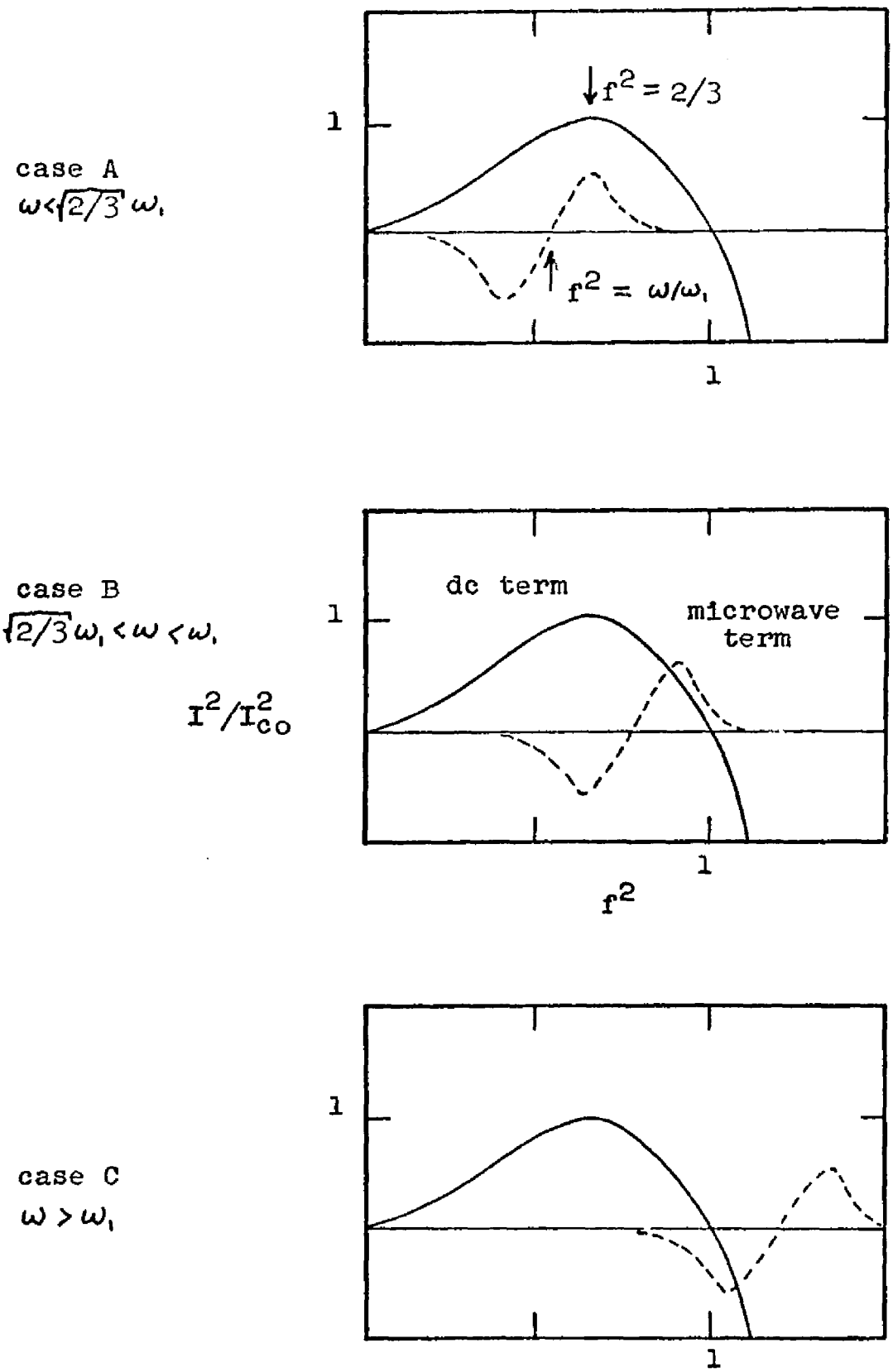

Figure 22. Free energy minimum relation between dc current and order parameter. For a given value of the order parameter, the dc current is the sum of the two terms plotted.

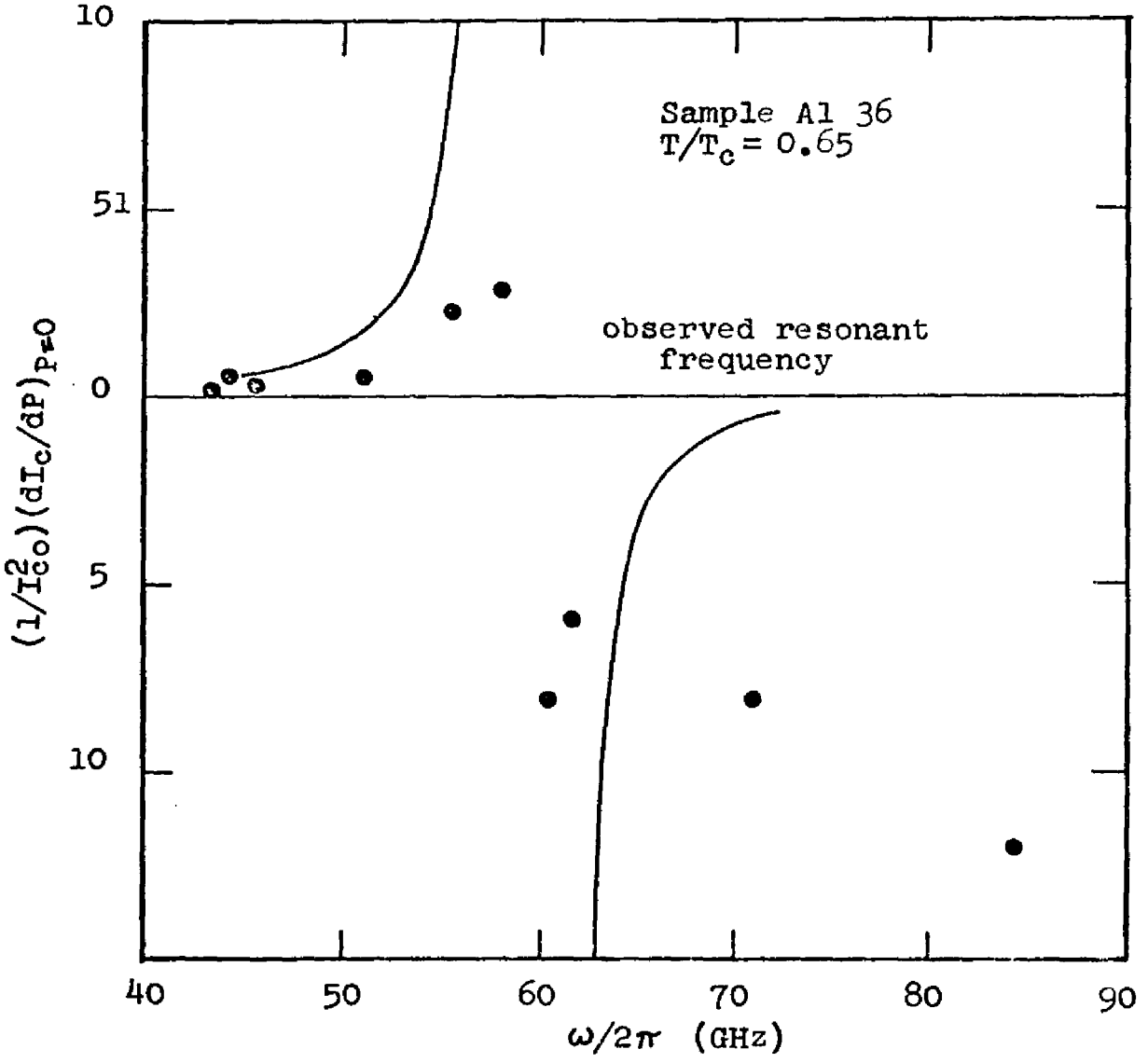

Figure 23. $(dI_c/dP)_{P=0}$ vs. ω.

entirely straightforward because ω_1 cannot be directly measured in the present experiment. As defined in this model, ω_1 is a small-signal resonant frequency corresponding to an unperturbed value of the order parameter. The experimentally observed resonance is measured at the rf critical current, where one would expect the order parameter to be somewhat depressed, i.e. $f < 1$. If we assume that for a critical rf current the order parameter has the same value as for the dc critical current, $f^2 = 2/3$, then the small signal enhancement predicted by IV-47 should change sign abruptly at the observed large signal resonant frequency. This assumption appears to be valid for the data shown in Figure 23.

The enhancement predicted is of the order of magnitude of the observed values, and the predicted frequency dependence is qualitatively correct.

The model explains why enhancement for $T = T_c$ is not observed in the aluminum dipoles. In the dipoles studied, for temperatures $\tau > 0.9$ the dipole resonance is heavily damped and no enhancement is predicted.

Implicit in the model is that no enhancement would be observed for microwave frequencies less than the inverse relaxation time of the order parameter.

The model has several serious shortcomings. In assuming a linear microwave response, we lose all information about critical microwave currents.

A more serious problem arises with the assumption of time averaging. In fact, the microwave frequencies used are

no more than a factor of two greater than the worst case predicted inverse relaxation time of the order parameter. While there may be a partial time-averaging, modulation of the order parameter by the microwave field certainly occurs, with effects not predicted by the model.

CHAPTER V

CONCLUSION

The observation of microwave enhanced critical currents at the beginning of experimental work motivated most of the subsequent work. In particular, considerable care was taken to obtain a thin film geometry with a well defined microwave response. The expectation that the enhancement mechanism would then be revealed has not been entirely fulfilled.

The model proposed provides an enhancement mechanism with many qualitative features observed experimentally. Consistent quantitative agreement with the model has not been obtained and cannot realistically be expected. The model is fairly crude in several respects, particularly in ignoring any microwave modulation of the order parameter.

A more adequate theoretical treatment might be difficult to achieve but is probably necessary for a definite determination of the enhancement mechanism. A better theory would probably enable direct experimental observation of the relaxation time of the superconducting order parameter.

REFERENCES

1. E. N. Economou and K. L. Ngai, Phys. Rev. Letters 20, 547 (1968).
2. P. W. Anderson, Phys. Rev. 112, 1900 (1958).
3. L. Onsager, private communication.
4. W. A. Little, Phys. Rev. 134, A1416 (1964).
5. G. E. Possin and K. W. Shepard, Phys. Rev. 171, 458 (1968).
6. R. Meservey and P. M. Tederow, J. Appl. Phys. 40, 2028 (1969).
7. R. E. Glover and H. T. Coffey, Rev. Mod. Phys. 36, 299 (1964).
8. T. K. Hunt, Phys. Rev. 151, 325 (1966).
9. J. Bardeen, Rev. Mod. Phys. 34, 667 (1962).
10. I. B. Bott, Proc. I.E.E.E. 52, 330 (1964).
11. J. Schneider, Phys. Rev. Letters 2, 504 (1959).
12. K. K. Chow and R. H. Pantell, Proc. IRE 48, 1865 (1960).
13. R. C. Wingerson, Phys. Rev. Letters 6, 446 (1961).
14. L. Holland, Vacuum Deposition of Thin Films (John Wiley and Sons, Inc., New York, 1960), pp. 143-164.
15. Op. cit., p. 344.
16. F. J. Low, J. Opt. Soc. Amer. 51, 1300 (1961).
17. P. L. Richards, J. Opt. Soc. Amer. 54, 1474 (1964).
18. M. R. Strongin, et al., Phys. Rev. Letters 21, 1320 (1968).
19. W. L. McMillan, Phys. Rev. 167, 331 (1960).
20. D. H. Douglas, Jr., Phys. Rev. 124, 735 (1961).
21. E. A. Lynton, Superconductivity (Spottiswoode, Ballantyne, & Co. Ltd., London, 1964) 2nd ed., pp. 109, 115.

22. D. C. Mattis and J. Bardeen, Phys. Rev. 111, 412 (1958).

23. R. E. Glover and M. Tinkham, Phys. Rev. 108, 243 (1958).

24. R. E. Glover and H. T. Coffey, Rev. Mod. Phys. 36, 299 (1964).

25. J. Bardeen, Rev. Mod. Phys. 34, 667 (1962).

26. P. G. DeGennes, Superconductivity of Metals and Alloys (W. A. Benjamin Inc., N. Y., N. Y., 1966), 1st ed., pp. 182, 184.

27. Op. cit., p. 130.

28. J. Gittleman, et al., Phys. Rev. 137, A527 (1965).

29. Handbook of Chemistry and Physics (Chemical Rubber Publishing Co., Cleveland, Ohio, 1959), 41st ed., p. 3257.

30. Op. cit., p. 3258.

31. Albert Schmid, Phys. Rev. 186, 420 (1969).

32. A. F. G. Wyatt, et al., Phys. Rev. Letters 16, 1166 (1966).

33. A. H. Dayem and J. J. Wiegand, Phys. Rev. 155, 419 (1967).

34. D. E. McCumber, Phys. Rev. 172, 427 (1968).